Energy Technology
Generation, Conversion, Storage, Distribution
www.entechnol.de

Review of Inorganic Hole Transport Materials for Perovskite Solar Cells

*Xin Jing, Zhuang Zhang, Tianyang Chen, and Jingshan Luo**

In the last decade, perovskite solar cells have witnessed great progress with a certified photoelectric conversion efficiency of 25.7%, which is comparable to single-crystal silicon solar cells, but the stability issue still restricts commercialization. As a solution to stability improvement, inorganic hole transport materials (HTMs) are widely studied due to their excellent stability compared to traditional organic HTMs, as well as low fabrication cost and high conductivity. Herein, the intrinsic properties of widely studied inorganic p-type materials for HTMs, their fabrication methods, and the progress that has been made with them are summarized. In addition, the cost of various inorganic HTMs is also discussed.

1. Introduction

1.1. Basic Knowledge of Hybrid Perovskite Solar Cells

Having been developed in the past decade, the highest certified efficiency of perovskite solar cells (PSCs) is now reaching 25.7%, which is close to that of traditional crystalline silicon cells (26.7%).[1] Furthermore, compared to silicon solar cells, PSCs have the potential advantages of being low-cost, light, flexible, semitransparent, and easy to fabricate (solution process, low temperature, etc.), which make PSCs a research hotspot in the photovoltaic field.[2]

Perovskite refers to a class of crystalline compounds adopting the generic chemical formula ABX_3, where A is a monovalent organic or metal cation (such as MA^+, FA^+, and Cs^+) at the center of the unit cell, B is a metal cation (generally Pb^{2+} and Sn^{2+}) with a smaller volume at the eight vertices of the cell, and X is a halogen anion (Cl^-, Br^-, and I^-) at the face center of the cell. Perovskite materials have some excellent properties, including a remarkably high absorption coefficient ($1.5 \times 10^4\ cm^{-1}$),[3] an absorption spectrum over the visible and near-infrared regions,[4] a low exciton-binding energy (≈16 meV),[5] a long charge-carrier diffusion length (>1 μm),[6] a high charge-carrier mobility ($25\ cm^2\ V^{-1}\ s^{-1}$),[7] a sharp optical band edge, and a tunable bandgap by replacing the cations and anions in the perovskite structure,[8] which make perovskites suitable for the absorber layers of highly efficient PSCs.

A typical PSC is usually composed of the following components: a perovskite absorber layer, which absorbs light, generates electron–hole pairs and separates charge carriers in the built-in electric field; transport layers, which can extract charge carriers and reduce carrier recombination; a metallic layer and a transparent conductive oxide (TCO) layer, which serve as conducting electrodes.[9] Considering whether electrons or holes are collected by the TCO layer, PSCs are classified as either conventional (n–i–p) or inverted (p–i–n) structures, as shown in **Figure 1**.

1.2. Roles of the Hole Transport Materials

A suitable hole transport material (HTM) should have primary requirements: 1) a high hole mobility to afford fast carrier extraction.[10] 2) An appropriate highest occupied molecular orbital (HOMO) (or valence-band) energy level to match the perovskite layer for hole transport and a proper lowest unoccupied molecular orbital (LUMO) (or conduction-band) to prevent electron leakage. The HOMO energy level of the HTM should lie above the valence-band energy of perovskite and the LUMO better lie above the conduction-band energy of perovskite.[11] 3) Good film-formation properties.[12] 4) High transparency (wide bandgap) in the visible spectrum to avoid the absorption screen effect of the active materials/absorbers.[13] 5) Good chemical, thermal, light, and water stability.[14] As a reference, HOMO (or valence band) and LUMO (or conduction-band) relative to the vacuum of several common transport layer materials and electrodes are illustrated in **Figure 2**. Furthermore, basic properties like hole mobilities and carrier concentrations of respective HTMs are summarized in **Table 1**. Specifically, different morphology, fabrication, or processing methods can lead to different results, so construction methods and device performances are also summarized in **Table 2**.

Traditionally, high-efficiency n–i–p structure PSCs are fabricated based on 2,2′,7,7′-tetrakis[N, N-di(4-methoxyphenyl) amino]-9,9′-spirobifluorene (spiro-OMeTAD). However, there are some obvious disadvantages of spiro-OMeTAD: 1) High cost

X. Jing, Z. Zhang, T. Chen, J. Luo
Institute of Photoelectronic Thin Film Devices and Technology
Solar Energy Research Center
Key Laboratory of Photoelectronic Thin Film Devices and Technology of Tianjin
Ministry of Education Engineering Research Center of Thin Film Photoelectronic Technology
Renewable Energy Conversion and Storage Center
Nankai University
Tianjin 300350, China
E-mail: jingshan.luo@nankai.edu.cn

The ORCID identification number(s) for the author(s) of this article can be found under https://doi.org/10.1002/ente.202201005.

DOI: 10.1002/ente.202201005

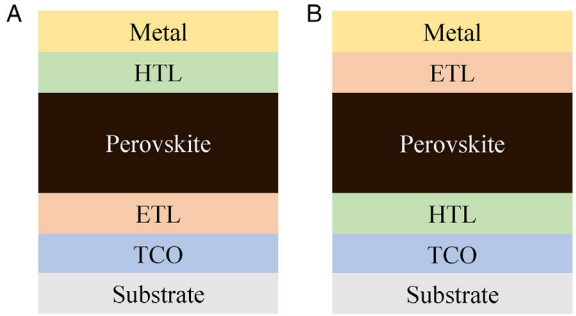

Figure 1. Perovskite solar cell (PSC) structures: A) n–i–p and B) p–i–n.

(≈5–7 times that of gold[17] according to commercial brand Sigma-Aldrich, due to the complex synthesis process). 2) Poor hole conductivity and mobility. Thus, extra additives such as bis(trifluoromethanesulfonyl)imide salt (Li-TFSI) and 4-tert-butylpyridine (tBP) are required to enhance the hole conductivity and mobility.[7] 3) Poor thermal stability. As the glass-transition temperature (T_g) of spiro-OMeTAD decreases significantly in the presence of additives, the amorphous nature of spiro-OMeTAD can easily induce crystallization under thermal stress.[99] Thus, Spiro-OMeTAD with additives was crystallized at 85 °C.[100] IV) Decreasing electrical properties. Ions in the perovskite layer diffusing into spiro-OMeTAD degrade the electrical properties of spiro-OMeTAD by decreasing charge-carrier collection ability through the formation of energy barriers.[101] V) Degrading hole transport layer (HTL) and perovskite layer. As a result of the deliquescent and hygroscopic nature of Li-TFSI, it can attract water molecules and cause quick degradation of the HTL as well as the perovskite film. Meanwhile, t-BP gives rise to the chemical decomposition of the perovskite by forming a [PbI_2·t-BP]-coordinated complex. Alternately, iodine may react with t-BP to form an iodopyridinate complex.[102]

Apart from spiro-OMeTAD, poly(triarylamine) (PTAA) is also used in the n–i–p structure, while poly (3,4-ethylene dioxythiophene) polystyrene sulfonate polymer (PEDOT: PSS) is usually applied in p–i–n structure. The superior performance of PTAA-based PSCs arises from the exceptional hole-mobility of PTAA ($\approx 4 \times 10^{-3}$ cm^2 V^{-1} s^{-1})[103] as compared to other polymers, as well as its strong chemical interaction with perovskites.[104] Especially, the device with PTAA has a photoelectric conversion efficiency (PCE) of over 23%.[105] However, PTAA also requires a dopant to further improve the conductivity,[106] of which the volatile nature also affects the stability of PSCs.[107] In addition, PTAA polymers are extremely expensive and their cost is ≈42–71 times that of gold according to commercial brand Sigma-Aldrich.[108]

In the p–i–n structure, PEDOT: PSS usually serves as an HTM. Some factors that contribute to its extensive use include the straightforward fabrication methods which can produce continuous and ultra-smooth films and the relatively good optical transparency (80–87%) and its high work function (WF) (≈5.1 eV).[24] However, PEDOT: PSS exhibits electrical inhomogeneity, great acidity, and hygroscopicity, which harms the long-term stability of PSCs, leading to some significant shortcomings.[109] 1) Degrading other layers. Due to its acidic nature, PEDOT: PSS can react with organic active layers, as well as etch the underlying transparent indium tin oxide (ITO) electrode, both of which limit the cell's long-term operational stability.[110]

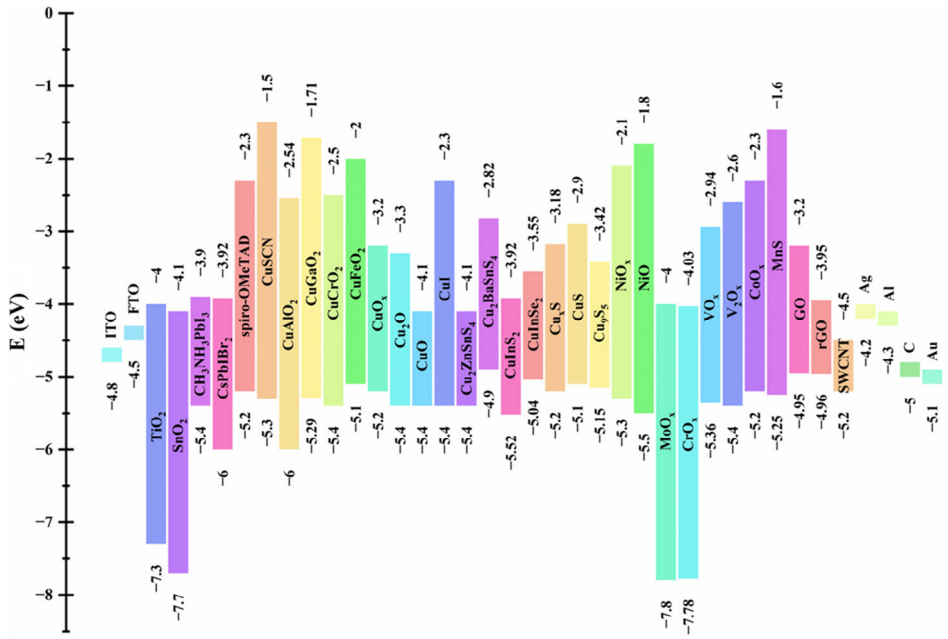

Figure 2. The highest occupied molecular orbital (HOMO) (or valence-band) and lowest occupied molecular orbital (LUMO) (or conduction-band) energy levels relative to the vacuum of common inorganic transport layers, perovskite layers, and electrodes. (The HOMO and LUMO of spiro-OMeTAD are also added for comparison.).

Table 1. Summary of the parameters of hole transport materials.

Material name	N [cm^{-3}]	μ [$cm^2 V^{-1} s^{-1}$]	Process condition
PEDOT: PSS	10^{21},[15]	0.045–1.7[15]	
PEDOT: PSS		10^{-5}–10^{-3},[16]	
Spiro-OMeTAD	7.13×10^{15},[17]	0.779[17]	
Spiro-OMeTAD		1.38×10^{-4},[18]	
Spiro-OMeTAD		10^{-5}–10^{-3},[19]	
Spiro-OMeTAD		1.4×10^{-6},[20]	
Spiro-OMeTAD		6.2×10^{-3},[21,22e]	
CuSCN		1.2×10^{-3}	
CuSCN	–	0.01–0.1[23,24b,25]	–
CuSCN	–	0.07	–
$CuAlO_2$	2.7×10^{19},[26]	10.4	
$CuAlO_2$	4.25×10^{15}–3.6×10^{18},[27]	11.3–39.5[27]	
$CuAlO_2$		3.6[28]	
$CuGaO_2$		0.23,[29]	
$CuGaO_2$		0.01–10	
$CuGaO_2$		0.1[22a]	
$CuGaO_2$	1.3×10^{18}	1.2×10^{-1}	Spin-coating film
$CuGaO_2$	6.3×10^{17}	7.3×10^{-2}	Spin-coating film
$CuGaO_2$	8.9×10^{17}	8.5×10^{-2}	Spin-coating film
$CuGaO_2$	3.098×10^{19}	3.81×10^{-2}	Spin-coating film
5% Zn: $CuGaO_2$	1.328×10^{20}	1.39×10^{-1}	Spin-coating film
$CuCrO_2$		0.1–1[30]	
$CuCrO_2$		0.59[31]	
$CuCrO_2$		3.81×10^{-2},[22d]	
$CuCrO_2$		10^{0}–10^{1},[22d]	
$CuFeO_2$	5.34×10^{18},[32]	0.59[22e]	
$CuFeO_2$		5.9×10^{-1},[22e]	
Cu_2O		100[33]	
Cu_2O		256[34]	
Cu_2O		0.49[35]	
CuO		0.129	
CuO	2.16×10^{19}	1.20×10^{-3}	Spin-coating Film
CuI		0.5–2[36]	
CuI		9.3[37]	
CuI	3.0×10^{19}	25[38]	Vacuum thermal evaporation film
CuI	5×10^{18}	6[39]	Solid–gas reaction film
CuI	1×10^{18}–1×10^{19}	0.5–2[40]	Spin-coating film
CuI	4.3×10^{16}	43.9[41]	Hydrothermal bulk crystal
Cu_2ZnSnS_4	5.6×10^{17}–1.85×10^{20},[42]	6-30[42]	
Cu_2ZnSnS_4		3.4×10^{-2},[43]	Spin-coating film
Cu_2BaSnS_4	3.0×10^{15}–1.2×10^{16},[44]	7.223[45]	
Cu_2BaSnS_4	1.18×10^{21},[46]	1.29[46]	
Cu_2BaSnS_4		1.36[47]	
$CuInS_2$		25[a],[48]	
$CuSbS_2$		49[a],[48]	
CuPc		10^{-2},[49]	
Cu_xS	1.37×10^{15},[50]	4.47[50]	
NiO_x	5.6×10^{16},[51]	4.7[51]	
		0.1[36]	
NiO		0.141[37]	
NiO	5.3×10^{18}	0.12[52b]	Spin-coating Film
NiO	$\approx 4 \times 10^{18}$	9[53]	Sputtering film
NiO	6.3×10^{14}–4.6×10^{18}	26–0.26[54]	Sputtering film
NiO_x			e-beam evaporation film
NiO_x			Spin-coating Film
Cu: NiO	7.3×10^{19}	2.53[52b]	Spin-coating Film
Cu: NiO	4.22×10^{20}	≈ 0.2[53]	Sputtering film
Cu: NiO	1.38×10^{14}–2.54×10^{20}	28.99–0.99[55]	Sputtering film
NiPc		1.9×10^{-4},[56]	
MoS_2	10^{16},[57]	200[57]	
MnS		0.45[18]	
GO		0.25[16]	
rGO		2–200[16]	
SWCNT		10000[58]	
MWCNT	1.94×10^{19},[59]	220[59]	
Carbon cloth embedded in carbon paste	5.178×10^{19}	3.67	

Note: N: hole concentration; μ: hole mobility; σ: conductivity. [a]The data is from the theoretical calculation.

2) Decreasing electric property. The semimetallic nature of PEDOT: PSS does not prevent electron flow to the anode.[24] 3) Poor chemical stability. Hygroscopicity, another significant and well-known negative of PEDOT: PSS, places restrictions on PEDOT: PSS-based cells' chemical stability in ambient conditions.[111]

Overall, traditional HTMs exhibit exceptional efficiency but they have other shortcomings, such as high cost and low stability.[112] Nevertheless, with moderate cost and conspicuous long-term stability, inorganic HTMs have emerged as promising alternatives to organic HTMs. Compared with organic HTMs, inorganic HTMs have superior advantages in these aspects: 1) Much lower cost in general. 2) Better stability and endurance in thermal and chemical terms. 3) Higher hole mobility. These advantages bring much more chances to large-scale commercial applications. Nowadays, the PSCs with some inorganic HTMs have already reached PCEs of over 20% and possessed much better stability than those with organic HTMs.[21]

Table 2. Construction methods and performances of inorganic HTL-based devices.

HTM	Method	V_{oc} [V]	J_{sc} [mA cm^{-2}]	FF [%]	PCE [%]	Stability PCE, time, (temperature, atmosphere, illumination)	References
CuSCN	Drop-casting	1.103	23.4	77.2	20.3	>85%, 1000 h, (85 °C, ambient, dark) >95%, 1000 h, (60 °C, ambient, 1 sun)	Arora et al. (2017)[21]
	Electrodeposition	1	21.9	75.8	16.6	>80%, 48 h, (RT, ambient, dark)	Ye et al. (2015)[60]
	Doctor blade	1.016	19.7	62	12.4	–	Qin et al. (2014)[61]
	Spin-coating	1.04	23.1	75.3	18.0	>60%, 2 h, (125 °C, 40% RH air, dark)	Jung et al. (2016)[62]
	Spin-coating [NH_3(aq.)]	1.10	22.7	71	17.5	>90%, 3 h, (–, N2, 1 sun)	Wijeyasinghe et al. (2017)[24b]
	Spray-coating	0.98	21.07	64	13.3	–	Liu et al. (2016)[17]
		1.013	23.10	73.1	17.0	94.2%, 100 d, (–, 30% RH air, –)	Yang et al. (2017)[63]
CuI	Spin-coating	0.99	22.6	71.3	16.0	93%, 288 h, (RT, 25% RH, –)	Sun et al. (2016)[64]
	Spin-coating [NH_3(aq.)]	0.99	19.37	74	14.21	90%, 15 d, (–, ambient, –)	Khadka et al. (2020)[65]
	Solid-–gas reaction	1.04	20.9	68	14.7	80%, 210 h, (–, air, –)	Wang et al. (2017)[66a]
	Interfacial reaction	0.85	22.99	47	9.24	≈94%, 30 d, (25 °C, 28 ± 2% RH air, –vv)	Nazari et al. (2017)[67]
	Spray–coating	1.03	22.78	0.75	17.60	92%, 90 d, (–, 40%–50% RH, –)	Li et al. (2017)[68a]
	Doctor blade	0.78	16.7	57	7.5	≈97%, 50 d, (–, N_2, –) ≈33%, 25 d, (–, air, –)	Sepalage et al. (2015)[69]
	Powder pressing	0.67	24.23	50	8.1	–	Uthayaraj et al. (2019)[70]
$CuAlO_2$/PEDOT: PSS	Sputter	0.88	21.98	75	14.52	≈80%, 240 h, (–, ambient, dark)	Igbari et al. (2016)[71]
$CuGaO_2$	Spin-coating	1.11	21.66	77	18.51	84.7%, 30 d, (25 °C, 30%–55% RH, –)	Zhang et al. (2016)[72]
5% Zn: $CuGaO_2$	Spin-coating	1.112	23.19	80.11	20.67	>95%, 60 d, (–, ambient, –) >85%, 1000 h, (85 °C, N2, –)	Chen et al. (2019)[22b]
$CuCrO_2$	Spin-cast	1.07	21.94	81	19.0	≈90%, 1000 h, (–, Ar, 5 mW cm^{-2} UV light)	Zhang et al. (2018)[22d]
$CuFeO_2$	Spin-cast	1.01	23.6	65	15.6	>85%, 1000 h, (–, N2, 1 sun, MPPT) >90%, 300 h, (–, 80 ± 5% RH, dark) ≈80%, 200 h, (60≈85 °C, 20% RH, dark)	Akin et al. (2019)[22e]
CuO_x	Solution-processed	1.11	22.5	75.8	19.0	–	Rao et al. (2016)[73]
Cu_2O	Solution-processed	1.07	16.52	75.51	13.35	>90% 70 d, (–, N2, –)	Zuo et al. (2015)[74]
	Sputter	0.96	15.8	59	8.93	–	Nejand et al. (2016)[33]
	Spin-coating	1.15	22.2	74.2	18.9	>90%, 30 d, (–, 30% RH air, –)	Liu et al. (2019)[75]
CuO	Solution-processed	1.06	15.82	72.54	12.16	–	Zuo et al. (2015)[74]
Cu_2ZnSnS_4 (CZTS)	Spin–coating	0.92	20.7	81	15.4	–	Khanzada et al. (2016)[43]
Cu_2BaSnS_4 (CBTS)	Sputtering	0.94	14.9	72	10.1	>90%, 30 min, (–, ≈70% RH air, –) ≈50%, 120 min, (–, ≈70% RH air, –)	Ge et al. (2017)[76]
$CuInSe_2$	Spin-coating	0.86	22.5	66	12.8	–	Zhang et al. (2019)[77]
NiO_x	Spin–coating	1.09	22.74	79.6	19.69	–	Chen et al. (2018)[78a]
F6TCNNQ: NiO_x	Spin–coating	1.12	23.18	80.3	20.86	–	Chen et al. (2018)[78a]
NiO_x	Spin–coating	1.07	20.58	74.8	16.47	–	Yin et al. (2016)[79a]
	Spin-coating (flexible)	1.04	18.74	68.9	13.43	–	
Cu: NiO	Spin–coating	1.12	22.28	81.2	20.26	≈95%, 1000 h, (23 °C, 50%–65% RH, –)	Chen et al. (2018)[52b]
Cu: NiO	Spin-coating(flexible)	1.10	21.45	73.8	17.41	–	
NiO	Spin-coating (precursor)	1.040	13.24	0.69	9.51	–	Wang et al. (2014)[80]
NiO_x	e-beam evaporation	1.06	18.6	77.8	15.4	–	Pae et al. (2017)[79b]
NiO	Screen-print	0.915	21.62	76	15.03	93%, 1000 h, (RT, 40% RH, dark)	Cao et al. (2015)[81]
NiO	Doctor blade	0.917	21.36	76	14.9	>93%, 1000 h, (RT, 40% RH air, dark) ≈20%, 150 h, (45 °C, 40% RH, 0.7 sun)	Xu et al. (2015)[82]

Table 2. Continued.

HTM	Method	V_{oc} [V]	J_{sc} [mA cm^{-2}]	FF [%]	PCE [%]	Stability PCE, time, (temperature, atmosphere, illumination)	References
	Drop-casting	0.912	22.84	76	15.8	>100%, 3000 h, (−, 15% RH, −)	Yang et al. (2016)[78b]
	Magnetron sputter	0.96	19.8	61	11.6	–	Wang et al. (2014)[51]
	Electrodeposition	0.936	14.9	75	7.26	–	Subbian et al. (2014)
	Spray pyrolysis	1.036	17.989	72.4	13.49	–	Chen et al. (2015)[83]
NiO	sol–gel-process	0.882	16.27	63.5	9.11	–	Zhu et al. (2014)[84b]
NiO	Atomic layer deposition ALD	1.04	21.87	72	16.40	–	Seo et al. (2016)[84a]
NiO	Pulsed laser deposition PLD	1.06	20.2	81.3	17.3	–	Park et al. (2015)[85]
$Li_{0.05}Mg_{0.15}Ni_{0.8}O$	Spray pyrolysis	1.10	23.09	81	20.65	–	Xie et al. (2017)[86]
$Li_{0.05}Mg_{0.15}Ni_{0.8}O$	Spray pyrolysis	1.083	20.4	82.7	18.3	97%, 1000 h, (−, −, dark) >90%, 1000 h, (−, −, 1 sun)	Chen et al. (2015)[87]
Cs: NiO_x	Spin–casting	1.120	21.77	79.3	19.35	98%, 70 d, (−, Ar, −)	Chen et al. (2017)[88]
MoO_x	Thermal evaporation	0.99	18.8	71	13.1	–	Liu et al. (2017)[89]
MoO_2	Scalable solvothermal cracking process	1.02	20.1	77.3	15.8	–	Im et al. (2017)[90]e
WO_x	Thermal evaporation	0.93	16.6	64	9.8	–	Tseng et al. (2016)[91a]
CrO_x	RF sputtering	0.93	14.9	67	9.27	–	Qin et al. (2016)[92]
	Radio frequency sputtering	1.03	20.17	71	14.76	–	Qin et al. (2018)[93]
Cu: CrO_x	RF sputtering	0.98	16.02	70	10.99	–	Qin et al. (2016)[92]
	Radio frequency sputtering	1.08	21.43	76	17.66	–	Qin et al. (2018)[93]
VO_x	Spin–coating	0.90	22.29	71	14.23	–	Sun et al. (2016)[91b]
CoO_x	Spin-coating	0.949	20.28	75.5	14.5	≈90%, 1000 h, (−, N2, dark)	Shalan et al. (2016)[91c]
GO	Spin-coating	0.943	19.5	75.1	13.8	>60%, 1000 h, (25 °C, 30% RH, −)	Jokar et al. (2017)[94]
rGO	Spin-coating	0.962	22.1	77.0	16.4	>50%, 1000 h, (25 °C, 30% RH, −)	Jokar et al. (2017)[94]
MnS		1.11	23.40	76.48	19.86	–	
P3HT/SWNTs-PMMA	Spin-coating	1.02	22.7	66	15.3	≈85%, 96 h, (80 °C, 62% RH air, −)	Habisreutinger et al. (2014)[95]
	Transfer	1.1	20.3	61	13.6		Aitola et al. (2016)[96b]
MWCNT	Drop-casting	0.88	15.6	75	10.3	≈90%, 10 d, (-, 20% RH, −)	Wei et al. (2015)[97]
Graphite	Drop-casting	0.93	10.30	64	6.13	–	Wei et al. (2015)[97]
carbon cloth	Carbon cloth embedded in carbon paste/Spiro-OMeTAD Doctor blade	1.12	20.42	67.0	15.29	≈90%, 16 h, (20 °C, N2, 1 sun, MPPT) ≈50%, 115 h, (20 °C, N2, 1 sun, MPPT)	Gholipour (2016)[98]

Note: V_{oc}: open-circuit voltage; J_{sc}: short-circuit current density; FF: fill factor; RH: relative humidity; RT: room temperature; MPPT: maximum power point tracking.

In this review, we provide comprehensive introductions of several promising inorganic HTMs which cover Cu-based HTMs, Ni-based HTMs, other transition metal oxides, as well as carbonaceous HTMs or electrode materials. We summarize their intrinsic properties (valence-band and conduction-band energy levels relative to the vacuum, hole mobilities, carrier concentrations, thermal and chemical stability, etc.), deposition processes, costs, and device performances based on corresponding HTLs. In addition, we shed perspective on the emergence of HTMs with better stability and conductivity to accelerate the commercialization of PSCs.

2. Basic Properties of Inorganic HTMs

2.1. Cu-Based Inorganic HTMs

2.1.1. Copper Thiocyanate (CuSCN)

Copper(I) thiocyanate (CuSCN) is an extremely cheap semiconductor. CuSCN crystallizes generally in two polymorphs, the orthorhombic (space group *Pbca*) α-phase and the hexagonal or rhombohedral β-phase.[113] Crystals of β-CuSCN exhibit

polytypism (i.e., variation in layer stacking order), consisting of 3 R and 2 H polytypes in syntactic coalescence along with some disorder and twinning.[113] The space groups are $R3m$ and $P6_3mc$, respectively. Pure crystals of both α- and β-CuSCN are practically colorless. The β-form always occurs as conical crystals with either a trigonal or a hexagonal base.[114] The β-CuSCN has layers of SCN ions separating the plains of Cu atoms and a strong Cu–S bond that interconnects three dimensionally,[115] whose polymer-like structure profits large thin-film deposition free of defects and pinholes.[116] Although some studies suggest that polymorphic systems containing both phases may be observed, thin films commonly exhibit the β-phase.[117]

The dominant p-type character of this material is explained in terms of copper vacancies.[117a] CuSCN is an intrinsic semiconductor, which can display p-type conductivity if the solid is created in a solution with a larger concentration of thiocyanate ions than copper ions. A stoichiometric deficiency of copper atoms is generated in the solid under this condition, and the hole transport character in p-CuSCN results from copper vacancies in the crystal lattice, with acceptor impurity levels produced close to the valence band maximum (VBM) of perovskites. Furthermore, because the removal of copper atoms from the perfect crystal lattice widens the optical bandgap, the copper defect structure also contributes to the optical transparency of the material. A stoichiometric surplus of copper atoms, in contrast, has the reverse effect and promotes higher n-type conductivity.[115,117b] The transistor devices constructed and evaluated in an inert environment were demonstrated to have intrinsic hole transport properties, but after being exposed to air for a few days, a considerable p-type-like doping impact was noticed. The characteristic energy shift toward the VBM was seen when some researchers measured the Fermi energy level after 1 h of exposure to ambient air, and they attributed this change to atmospheric p-doping.[23] It is reported that exposure to ambient air causes a reversible and inadvertent p-doping of CuSCN. After being exposed to ambient air for 7 days, there was no change in the VBM energy of the CuSCN layers, demonstrating that CuSCN retains its stability.[24b] CuSCN's hole transport properties are also known to be substantially influenced by manufacturing conditions, device geometry, electrode contact resistance, and dielectric/semiconductor interface trap density in addition to extrinsic doping effects.[23]

CuSCN exhibits a wide bandgap of ≈3.8 eV (The VBM and conduction band minimum (CBM) energy levels are −5.3 and −1.5 eV relative to the vacuum, respectively.),[60] remarkable optical transparency (98% transmission at 390–750 nm,[118] 89% transmission at 400–1300 nm[24a]), high hole mobility ($0.01 \approx 0.1\ cm^2\ V^{-1}\ s^{-1}$).[23] Also, CuSCN processes inherently high thermal stability at elevated temperatures. Jung et al. reported that CuSCN heat-treated in the air at 200 °C for 1 h still does not degrade and both oxygen and moisture in the ambient environment do not influence significantly CuSCN thermal degradation.[62] Ptaszyński et al. pointed out that the decomposition of CuSCN into copper sulfide is only observed at temperatures above 300 °C.[119] It is mentioned that CuSCN shows extraordinary chemical stability resulting from the polymeric nature of the solid.[120]

The use of CuSCN as the HTMs has been demonstrated in numerous emerging opto/electronic applications including thin-film transistors (TFTs) and integrated circuits,[118,121] organic photovoltaic (OPV) cells,[24a,122] hybrid PSCs,[9–11] organic light-emitting diodes (OLEDs),[123] water oxidation (as a superior photocatalyst),[124] and dye-sensitized photocathodes.[125]

2.1.2. Copper Iodide (CuI)

CuI is an environment-friendly material composed of nontoxic and naturally abundant elements. CuI undergoes multiple polymorphic phase transitions during heating: γ (zinc blende structure, space group $F43m$)→ β (wurtzite structure, $P6_3mc$)→ α (rock salt structure, $Fm3m$) at 643 and 673 K,[126] respectively. (Also some articles say critical phase temperatures are 623 and 665 K[127] or 642 and 680 K.[128]) The cubic α-CuI is a mixed conductor. The hexagonal β-CuI is an ionic conductor. The cubic γ-CuI is a p-type I–VII semiconductor and stable at room temperature, whose conductivity originates from the copper vacancies or the presence of iodine in stoichiometric excess.[127]

The γ-CuI processes many excellent properties: wide direct bandgap of ≈3.1 eV (The VBM and CBM energy levels are −5.4 and −2.3 eV relative to the vacuum, respectively.),[64] high exciton-binding energy (62 meV),[41] high optical transparency (i.e., 80% at 400–900 nm deposited by pulse laser[129]; 90% at 410–1500 nm deposited by thermal evaporation),[38] high hole mobility of $25\ cm^2\ V^{-1}\ s^{-1}$, hole concentration of $3.0 \times 10^{19}\ cm^{-3}$, and low resistivity of $1 \times 10^{-2}\ \Omega\ cm$.[38] The coordination chemistry of CuI makes it readily coupled with many inorganic and organic ligands. It is also an attractive inorganic precursor to coordination clusters and polymers supported by various organic ligands for photochemical, photophysical, and other applications.[130]

CuI is stable at room temperature[131] but the thermal stability of CuI still needs to be improved. It is reported that higher heating temperatures over 350 K frequently lead to the degraded electrical conductivity of γ-CuI, considering the diffusion of iodine (and other defects) in γ-CuI thin films during heat treatment.[132] Zi et al. believed that the evaporation of a trace amount of iodine fr963.om CuI film due to the high substrate temperature (>120 °C), and decreasing the concentration of copper vacancies (V_{Cu}) is the key reason for degrading the CuI film's semiconductor physical properties.[38] Hence, a capping (protective) layer is required to improve the thermal stability of γ-CuI thin film at further elevated temperatures. For example, Yang et al. significantly suppress the degradation of the conductivity of γ-CuI thin film during air-annealing by capping with a CuO_x layer.[132] By the way, it is reported that CuI film will turn into CuO film by heating CuI film in the air at high temperatures (>300 °C).[74]

After being exposed to ambient humidity for 5 h, a twofold rise in the conductivity of CuI is observed, followed by a little long-term deterioration. The WF of CuI also lowers simultaneously by about 1 eV. The conductivity gain is maximal at middle humidity levels and is partly reversible. Andrea Crovetto et al. propose that hydration of grain boundaries may benefit the overall hole mobility based on the significant intragrain mobility detected by THz spectroscopy.[133]

CuI is applied in electronic devices such as highly efficient light-emitting diodes,[134] photodiode detectors,[135] and transparent flexible thermoelectric materials.[132] CuI thin films also have vast potential in solar cells as promising HTLs in PSCs, as buffer layers in $CuInX_2$ (X = S, Se, and Te)-based solar cells,[136] as

versatile hole-selective contact for organic solar cells,[137] and to replace the liquid electrolyte in dye-sensitized solar cells (DSSC) (construct a fully solid-state dye-sensitized photovoltaic cell).[138]

2.1.3. Copper Oxides (CuO_x): CuO, Cu_2O

Stable copper oxides (CuO_x), namely, cupric oxide (CuO) and cuprous oxide (Cu_2O), are well-known p-type semiconductors. (The VBM and CBM energy levels of CuO_x are −5.2 and −3.2 eV relative to the vacuum, respectively.[73] Those of Cu_2O are −5.4 and −3.3 eV, and those of CuO are −5.4 and −4.1 eV.[74]) Due to the natural abundance of copper and oxygen, CuO_x is a promising alternative for photovoltaic systems. Cu_2O can react with O_2 and form CuO after being heated at 250 °C in air. CuO film can also be obtained by heating CuI film in the air under high temperatures (>300 °C).[74]

2.1.4. Delafossite: $CuAlO_2$, $CuCrO_2$, $CuGaO_2$, and $CuFeO_2$

$CuAlO_2$, $CuCrO_2$, $CuGaO_2$, and $CuFeO_2$ are known to be the delafossite structure with a general formula of ABO_2, where a sheet of linearly coordinated A cations is stacked between edge-shared octahedral BO_6 layers, and have been investigated as p-type semiconductors. The mobility of these ternary copper compounds is in the range of 0.1–10.4 $cm^2 V^{-1} s^{-1}$. This value is close to that of the p-doped GaN (about 10 $cm^2 V^{-1} s^{-1}$).[41] Because of their decent optical transparency, chemical and thermal stability, and natural abundance, they are very promising HTM candidates for improving photovoltaic performance, device stability, and fabrication of low-cost cells. They can be manufactured in PSCs by sputtering,[71] spin-coating,[22] etc.

$CuAlO_2$ has been reported to possess decent optical transparency, chemical and thermal stability, a low-cost preparation process, and nontoxic elements. Its conductivity could also be as high as 1 S cm^{-1}. Igbari et al. fabricated 15 nm $CuAlO_2$ HTL by sputtering (a homogeneous, compact, and continuous morphology is achieved; in the 400–800 nm spectrum range, transmission is ≈80%.) with the best PCE of 14.52%.[71]

$CuGaO_2$ has been investigated extensively as a photocathode in the p-type dye-sensitized solar cell. It shows good optical transparency (due to its large bandgap of 3.58 eV), proper low-lying VBM (≈−5.3 eV), and high hole mobility ($10^{-2} \approx 10^{1}$ $cm^2 V^{-1} s^{-1}$), which shows PSCs potential to rival inorganic photovoltaics based on silicon, cadmium telluride, and copper indium gallium selenide.[22b,72]

$CuCrO_2$ has been extensively investigated in p-type dye-sensitized solar cells and organic solar cells. In particular, as an alternative to the typically used NiO_x HTL, it has delivered superior performance due to the higher electrical conductivities and more negative VBM. Its VBM and CBM energy levels are −5.4 and −2.5 eV, respectively. $CuCrO_2$ has >70% transmittance in the wavelengths across 400–800 nm. More importantly, the bandgap of $CuCrO_2$ is about 2.9 eV, enabling a broad absorption in the UV region while maintaining high transmittance in the region of wavelengths above 400 nm. This feature is of great relevance as a UV-blocking underlayer to retard the decomposition of perovskite materials without obviously attenuating the light-harvesting in the rest of the solar spectrum.[22e]

2.1.5. Kesterite: Cu_2ZnSnS_4 (CZTS), Cu_2BaSnS_4 (CBTS)

Kesterite Cu_2ZnSnS_4 (CZTS) is considered one of the high-potential material systems for solar energy production considering its nontoxicity, direct bandgap (with the optimal bandgap of 1.5 eV, high absorption coefficient ($\approx 1 \times 10^4$ cm^{-1}), and excellent environmental stability. The conventional process for CZTS deposition is based on high vacuum processes which are highly capital-intensive. The development of non-vacuum deposition processes may substantially reduce production costs. These non-vacuum processes such as spray pyrolysis, electrodeposition, sol–gel, and nanoparticles or colloidal route of synthesis are more attractive for scaling-up production.[43]

A wide bandgap (≈2.04 eV) p-type quaternary chalcogenide Cu_2BaSnS_4 (CBTS) semiconductor is demonstrated as a promising HTM owing to its satisfactory chemical and thermodynamic stability, high carrier mobility (≈10 $cm^2 V^{-1} s^{-1}$), and suitable band alignment with perovskite.[76]

2.1.6. Chalcopyrite: $CuInSe_2$ (CISe)

Some Cu-based chalcopyrite semiconductors, such as $CuInS_2$, have been applied to PCSs as inorganic HTMs. Among them, $CuInSe_2$ shows great potential for HTM because of its high absorption coefficient, tunable bandgap, low toxicity, simple preparation, and low cost.[77] Its VBM and CBM energy levels are −5.04 and −3.55 eV relative to the vacuum, respectively.[77]

2.2. Nickel Oxide (NiO_x)

NiO_x includes NiO, Ni_2O_3, and NiOOH. The as-prepared NiO is nonstoichiometric and thus is noted as NiO_x.[79] NiO is a wide bandgap p-type oxide semiconductor and has the potential for applications in solar energy conversion as an HTM. It also has good optical transparency and high chemical stability, and the capability of aligning the band edges to the perovskite layers. The cubic rock-salt NiO crystal structure is in the space group *Fm*3*m* (NaCl-type).[84] Its VBM and CBM energy levels are −5.5 and −1.8 eV relative to the vacuum, respectively, and the Fermi level (E_f) of the NiO NCs is even higher (−5.36 eV).[84b] The wide-bandgap semiconductor NiO in its stoichiometric form has a relatively low intrinsic conductivity, while the often-seen p-type conductivity in undoped NiO is typically attributed to the nickel vacancies VNi. Because the Ni vacancies have high ionization energy, the hole density in undoped NiO is constrained.[139] The low hole transfer efficiency of intrinsic NiO would result in hole accumulation near the perovskite interface and hence a large possibility of electron-hole recombination at the NiO-perovskite interface,[140] but it can be increased by extrinsic dopants with more shallow acceptor levels,[139] such as Cs: NiO_x,[88] Cu: NiO_x,[52] etc.

2.3. Other Transition Metal Oxides

Other transition metal oxides including CrO_x, MoO_x, VO_x, CoO_x, and WO_x, have been used as HTMs in PSCs because of their wide bandgap, high stability, high WF, and good hole transport properties. The main construction method for MoO_x, CoO_x,

VO_x, and WO_x is spin-coating.[91] For CrO_x, radio frequency (RF) sputtering[92] is more often used. CrO_x doped by Cu (Cu: CrO_x)[93] boosts the efficiency compared with the pristine. The VBM and CBM energy levels of CrO_x are −7.78 and −4.03 eV relative to the vacuum, respectively.[92] As an amorphous complex containing Cr^{3+}, Cr^{4+}, and Cr^{6+} oxidation states at 200 °C, CrO_x thin film exhibits p-type semiconducting behavior due to the predominance of chromium vacancies as defects.[141] Cr_2O_3 is extremely stable and can withstand harsh oxidizing conditions, including aqua regia.[92,142] The VBM and CBM energy levels of MoO_x are −7.8 and −4 eV relative to the vacuum, respectively.[89] Among MoO_x, particularly, MoO_3 is a very promising material since it is nontoxic and has deep-lying electronic states, with a WF of 6.7 eV for vacuum-deposited MoO_3 (unexposed) and 5.5 eV for air-exposed MoO_3.[143] The VBM and CBM energy levels of VO_x are −5.36 and −2.94 eV relative to the vacuum, respectively.[91b] Those of V_2O_x are −5.4 and −2.6 eV.[144] It is discovered that VO_x's bandgap's defective states are critical for lowering the energy barrier for hole transportation injection.[145] The VBM and CBM energy levels of CoO_x are −5.2 and −2.3 eV relative to the vacuum, respectively.[91c] Cobalt has characteristics with nickel as another member of the iron family. CoO_x has a narrower bandgap than NiO_x, which contributes to its lower transmittance. The conductivity of CoO_x is also inferior to NiO_x. So, in some cases, doped-CoO_x is adopted.[63] In general, devices built of metal-oxide HTM have shown exceptional long-term durability in tests of performance stability in air.[91c]

2.4. Carbonaceous HTMs

Carbonaceous materials can act as both counter electrodes and as HTLs. Carbonaceous materials such as graphene oxide (GO), reduced-graphene oxide (rGO), and carbon nanotubes (CNTs, including single-walled carbon nanotubes (SWCNTs) and multi-walled carbon nanotubes (MWCNTs)) are being used as HTMs or electrodes in PSCs. Carbonaceous materials have low cost, good connectivity, and the unique property of exhibiting good mechanical performance and adhesion to the film, which will reduce the interface resistance in solar cells.[146]

2.4.1. GO and rGO

GO and rGO, which have a 2D sheet structure consisting of a carbon atom monolayer, are considered to have great potential to be used in PSCs as they exhibit good electrical conductivity and high specific surface area.[94,146a] The Hummers method can be used to create GO, an oxidized version of graphene, from graphite. This approach comprises chemical oxidation using strong sulfuric and nitric acid, $KMnO_4$, and H_2O_2, followed by sonication and exfoliation.[147] In contrast to hydrophobic pristine graphene, which has a large surface area, good heat transfer, and electrical conductivity, GO has great hydrophilicity, allowing it to disperse in polar solvents and be functionalized for use in hybrid materials based on graphene.[148] Low temperature and solution processing of thin films are made possible by the creation of such graphene dispersions in solvent media. However, because GO is electrically insulating, its electronic characteristics are inferior to those of graphene. Reduction to remove a sizable portion of the oxygenated moieties can further modify this to restore both electrical and thermal conductivities. rGO is the common name for such a graphene derivative.[94] GO made from the Hummers method was reduced with reagents such as hydrazine (N_2H_4), sodium borohydride ($NaBH_4$), or 4-hydrazino benzenesulfonic to produce rGO.[94,149]

The VBM and CBM energy levels of GO are −4.95 and −3.2 eV relative to the vacuum, respectively.[150] The hole conductivity of GO is 10^{-5} S cm^{-1}, and the hole mobility (μ_h) of GO is 0.25 cm^2 V^{-1} s^{-1}.[16] GO film (9 nm) processes high optical transparency of ≈96% for 550 nm light.[151] GO film resistance is 4.3×10^4 Ω square^{-1}.[152] The VBM and CBM energy levels of rGO are −4.96 and −3.95 eV relative to the vacuum, respectively.[149] The hole conductivity of rGO is $0.05 \approx 4$ S cm^{-1}, and hole mobility (μ_h) of rGO is $2 \approx 200$ cm^2 V^{-1} s^{-1}, which, because of residual groups and defects, is higher than GO but lower than graphene.[148] rGO films with sheet resistances as low as $10^2 \approx 10^3$ Ω square^{-1} and optical transmittances above 80% for 550 nm light are achieved through thermal annealing. The film conductivity of rGO typically decreases inversely as optical transmittance rises.[153]

In terms of thermal stability, Tang et al. reported that according to thermogravimetric curves, the mass loss for GO starts above room temperature, while at 258 °C, the mass loss reaches the peak.[154] From room temperature to 200 °C, the absorbed water molecules evaporate and cause a modest reduction in the weight of GO. This weight loss is then compounded by the breakdown of oxygen-containing functional groups, losing a total of about 60% of its mass up to 600 °C. However, rGO exhibits superior thermal stability, losing in total just around 9% of its mass up to 600 °C. rGO has much higher thermal stability as a result of the chemical reduction that removes the thermally labile oxygen functional groups.[16,155]

2.4.2. Carbon Nanotubes (SWCNTs and MWCNTs)

Carbon nanotubes are capable of efficiently extracting photo-generated charges and enhancing the resilience and durability of a PSC. These attributes include excellent charge transport capabilities, chemical inertness, and mechanical robustness.[98] The VBM and CBM energy levels of GO are −5.2 and −4.5 eV relative to the vacuum, respectively.[156] The WF of MWCNTs is 4.6 eV.[157] CNTs-based contacts offer also other important advantages, such as extremely high flexibility and semitransparency, which are required in, for example, bifacial solar cells. Also, they can serve as an interface layer.[158]

3. Preparation and Deposition of the Inorganic HTMs

3.1. Cu-Based Inorganic HTMs

3.1.1. Copper Thiocyanate (CuSCN)

CuSCN film can be made by successive ionic layer adsorption and reaction (SILAR) (however, this method leads to a rough surface),[159] inkjet-printing (this method leads to the formation

of large discontinuities in the film, which in turn results in poor device performance),[160] electrodeposition,[161] etc.

CuSCN HTM can be achieved by drop-casting,[21] doctor blading (this method produces a thick CuSCN layer with ≈1 μm thickness),[61] electrodeposition ($CuSO_4$, potassium thiocyanate, ethylenediaminetetraacetic acid, solution deposition),[60] spin-coating,[62,162] and spray-coating,[17,24b,63] etc. Among them, spin-coating, drop-casting, and spray-coating achieved better performance of devices. Despite the simplicity, spin-coating of CuSCN is still challenging as it is largely insoluble in the vast majority of common solvents. A handful of n-alkyl sulfide solvents are known to dissolve CuSCN at appreciable concentrations, such as dimethyl sulfide,[24a] propyl sulfide,[117a] and diethyl sulfide,[21] etc. (While reports on alternative organic solvents such as dimethyl sulfoxide do exist, the power conversion efficiencies achieved have been limited [<5% in organic solar cells] by the high surface roughness of the resulting CuSCN layer.[24b]) These sulfur-based solvents are highly polar solvents, which can arguably damage the underneath perovskite layer in the n–i–p structure. Therefore, to minimize the interaction between perovskite and diethyl sulfide solvent, Arora et al. dynamically used a drop-cast deposition approach in which the solvent evaporated rapidly as compared to the conventional deposition approach. As a result, a high PCE of 20.3% is yielded and maintains >85% PCE after 1000 h in ambient conditions in the dark at 85 °C (**Figure 3**), whose PCE is close to the PSCs with Spiro-OMeTAD and stability is much better than the latter.[21] Similarly, spray-coating, which allows the solvent to evaporate instantly to form a crystallized CuSCN layer without any significant damage to the underlying perovskite layer, is also reported with a PCE of 17.10%.[63] In addition, CuSCN can be dissolved in ammonium hydroxide. Ultrathin (3–5 nm) layers of CuSCN are formed when the aqueous CuSCN–ammine complex solution is spin-cast in air and annealed at 100 °C.

In p–i–n structure, CuSCN layers processed from NH_3(aq) solutions exhibited high compositional purity, exceptional surface uniformity, and superior substrate planarization properties, reaching a PCE of 17.5%.[24b] The processing versatility of CuSCN enables its combination with inexpensive, and often temperature-sensitive, substrate materials such as plastic.[163]

3.1.2. Copper Iodide (CuI)

CuI thin films have been prepared by several techniques, such as SILAR,[164] chemical bath deposition,[159a] electrochemical deposition (grow highly oriented CuI thin films onto ITO glass substrate),[165] pulsed laser deposition (PLD, CuI films exhibit excellent transparent conductive properties and highly crystallized and (111) orientation),[166] thermal evaporation,[38] and sputtering.[167] The sputtering technique at room temperature can be upscaled for producing large-area transparent CuI thin films on low-cost flexible and transparent substrates.[132] Among these thin-film growth techniques, sputtering, PLD, and thermal evaporation have yielded better physical properties of CuI thin films such as low resistivity and high optical transmission. However, γ-CuI films produced by the vapor iodination method usually have very rough surface morphology leading to a frosted-glass-like appearance, rendering them far from truly

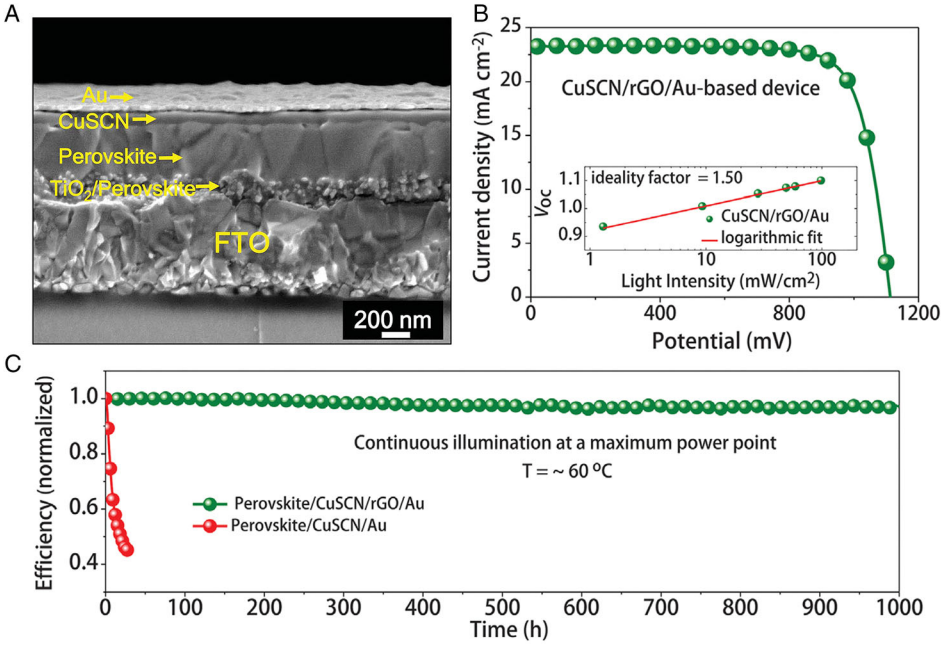

Figure 3. Typical n–i–p structure (CuSCN) device performance. A) Top-view scanning electron microscope (SEM) image of the perovskite film deposited onto mesoporous TiO_2; perovskite grains are visible. B) Current density–voltage curve of the CuSCN-based device recorded at a scan rate of 0.01 V s^{-1}; the inset shows the open-circuit voltage (V_{OC}) as a function of illumination intensity with an ideality factor of 1.50. C) Operational stability of an unencapsulated CuSCN-based device with and without a thin layer of reduced-graphene oxide (rGO, as a spacer layer between CuSCN and gold layers), examined at a maximum power point under continuous full-sun illumination at 60 °C in a nitrogen atmosphere. Reproduced with permission.[21] Copyright 2017, The American Association for the Advancement of Science.

transparent thin films. This is a crucial issue that must be resolved for application in transparent electronics. γ-CuI films with shiny surfaces can be directly deposited from bulk γ-CuI by using physical vapor deposition (PVD) techniques such as thermal evaporation, sputtering, and PLD.

The CuI transport layer can be produced by dissolving the CuI powder into dipropyl sulfide, acetonitrile, or propyl sulfide to spin-coating[64,137b] or spray-coating.[68] Li et al. spray-coated 60 nm (30–90 nm) CuI with a PCE of 17.6%. It can retain approximately 92% of its initial efficiency even for 90 days, much better than 20% of spiro-MeOTAD for 50 days.(**Figure 4**a)[68a] Nazari et al. used an interfacial reaction method with thermal evaporation of 120 nm of Cu on the perovskite layer containing an excess amount of methylammonium iodide (MAI) on the top of the surface, which obtain a PCE of 9.24%.[67] Through the doctor blade, the CuI layer was deposited by the doctor blading a solution of CuI in a di-n-propyl sulfide/chlorobenzene solvent mixture under ambient conditions. The CuI layer used in this study was approximately 400 nm thick and consisted of small particles that are connected to form a 3D structure. The CuI surface was found to be rough and showed gaps between particles, resulting in a PCE of 7.5%.[69] Uthayaraj et al. achieved a device of 8.1% PCE through a powder-pressing approach.[70]

In p–i–n structure, Sun et al. spin-coated 30 nm CuI film with a PCE of 16.0%. It can retain approximately 93% for 288 h in the air at 25% humidity and room temperature.[64] Khadka et al. employed CuI deposited with ammoniated aqueous solution ink as HTL to spin-coating and annealing with a PCE of 14.21%.[65] Wang et al. used a solid–gas reaction, iodination of Cu films, to fabricate a uniform CuI film by exposing a thermally evaporated copper film to iodine vapor with a PCE of 14.7%.[65,66]

In the p–i–n structure, Rao et al. deposited ultrathin CuO_x film (about 5 nm) whose PCE has reached as high as 19.0% using the solution-processed method.[73] Zuo et al. used a solution-processed method (Cu_2O film was prepared via in situ conversion of CuI film in aqueous NaOH solution. CuO film was made by heating Cu_2O film in the air.) and PCEs of 13.35% and 12.16% were achieved for Cu_2O and CuO cells, respectively. In the 400–1000 nm spectrum range, the transmittance for 10 nm thick Cu_2O is above 93% and 10 nm thick CuO is above 97.5%.[74]

3.1.3. Copper Oxides (CuO_x): CuO, Cu_2O

The CuO_x preparation methods include solution process,[73,168] sputtering,[33] spin-coating[75] and spin-coating precursor solution,[73] etc. Traditional methods for making Cu_2O film are electrodeposition, thermal oxidation, sputtering, and metal–organic chemical vapor deposition.[74] These methods are complicated and costly, requiring advanced equipment. Liu et al. spin-coated Cu_2O ink whose Cu_2O nanoparticles are dispersed in solution and the PCE maintain over 90% of their initial 18.9% efficiency after 30 d when stored in ambient air without encapsulation.

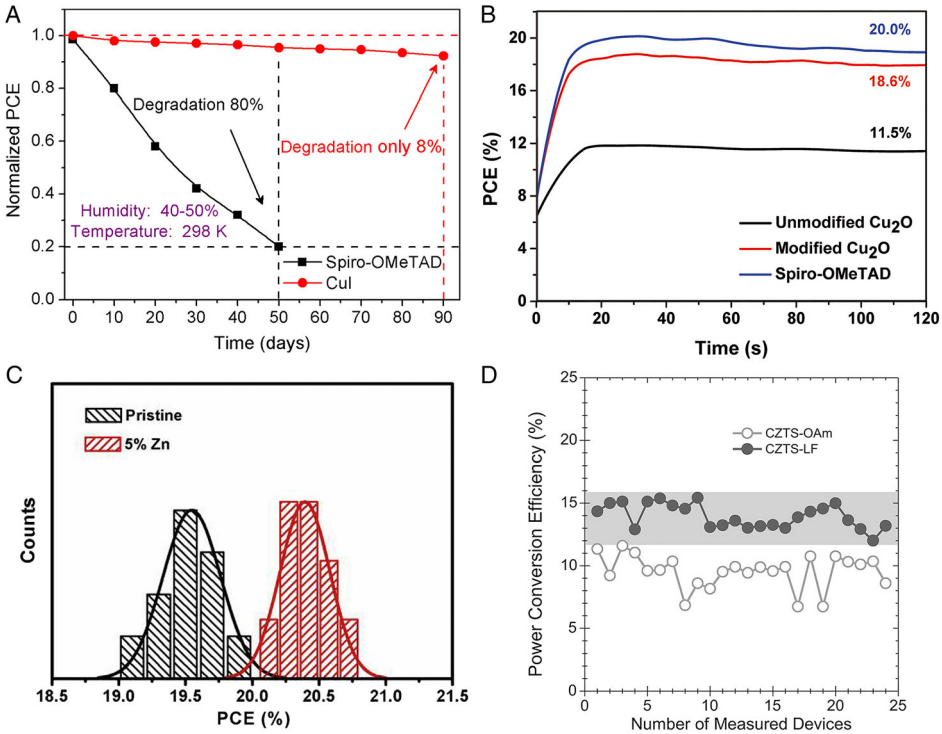

Figure 4. A) Normalized photoelectric conversion efficiency (PCE) changes of both spiro-OMeTAD and CuI-based PKSCs. Reproduced with permission.[68a] Copyright 2017, American Chemical Society. B) MPP tracking for 120 s to yield a stabilized efficiency for unmodified Cu_2O, modified Cu_2O, and Spiro-OMeTAD-based devices. Reproduced with permission.[75] Copyright 2019, John Wiley and Sons. C) Histogram distribution of the device efficiencies based on the pristine and 5% Zn: $CuGaO_2$ hole transport materials (HTM). Reproduced with permission.[22b] Copyright 2019, Elsevier. D) Histogram of the solar cell efficiencies obtained from 24 samples employing OAm-capped Cu_2ZnSnS_4 (CZTS) and CZTS-LF as HTLs, respectively. Reproduced with permission.[43] Copyright 2016, John Wiley and Sons.

A straightforward surface modification technique that makes use of a silane coupling agent is suggested for producing stable and inexpensive cuprous oxide (Cu_2O) quantum dots. To retain an n–i–p structure, the modified Cu_2O can be directly deposited as the top HTL on the perovskite layer. When using surface-modified Cu_2O as the HTL, PSC efficiency is much greater (18.9%) than when using unmodified Cu_2O (11.9%). (Figure 4b)[75] Zuo et al. reported a solution-processed CuO HTL with a PCE of 12.16%.[74]

3.1.4. Delafossite: $CuAlO_2$, $CuCrO_2$, $CuGaO_2$, and $CuFeO_2$

In the n–i–p structure, Zhang et al. spin-coated $CuGaO_2$ nanoparticles, through which the resulting PCE of optimum devices was 18.51%.[72] Zhang et al. spin-coated the solution of $CuCrO_2$ nanocrystals at low temperature processed as an about 45 nm thickness compact HTL with the best PCE of 19.0%, which can maintain ≈90% PCE after 1000 h kept in an Ar-filled dry glove box.[22d] Akin et al. spin-coated $CuFeO_2$ nanoparticles dispersed in solution and received the best PCE of 15.6%. They synthesized $CuFeO_2$ using a hydrothermal reaction at 130 °C and spin-coated $CuFeO_2$ nanoparticles dispersed in absolute isopropanol, then dried.[22e]

In p–i–n structure, Igbari et al. fabricated 15 nm $CuAlO_2$ HTL using sputtering to achieve a homogeneous, compact, and continuous morphology, whose transmission is about 80% in the 400–800 nm spectrum range, with the best PCE of 14.52%.[71] Chen et al. dispersed $CuGaO_2$ nanocrystals in paste and spin-coating. The mesoporous (Zn^{2+}-doped) $CuGaO_2$ films can be obtained after annealing at 350 °C for 30 min to burn off the organic. As a result, devices with pristine $CuGaO_2$ achieved the best PCE of 20.00%, and devices with Zn^{2+}-doped $CuGaO_2$ achieved the best PCE of 20.67%. The latter can maintain >95% PCE in 60 d at ambient conditions; >85% PCE at 85 °C for 1000 h in a nitrogen atmosphere (Figure 4c).[22b]

3.1.5. Cu_2ZnSnS_4 (CZTS), Cu_2BaSnS_4 (CBTS), $CuInSe_2$

Khanzada et al. spin-coated "ligand-free" CZTS nanoparticle ink with the best device PCE of 15.4%. Engineering the surface ligands of CZTS nanocrystals produces high-purity CZTS nanocrystals. (Figure 4d)[43] Similarly, Zhang et al. achieved a 12.8% PCE device through spin-coating $CuInSe_2$ nanoparticle ink. Ge et al. sputtered 100 nm thick CBTS HTL with the best PCE of 10.1%.[76]

3.2. Carbonaceous HTMs

Carbon-based materials can be easily prepared by simple techniques such as spin-coating, doctor blading, and screen-printing.[146] Carbon nanotubes (SWCNTs and MWCNTs) layers are fabricated by transferring,[96] spin-coating,[95] coating,[97,156] and screen-printing.[169] GO, rGO can be spin-coated[170] or

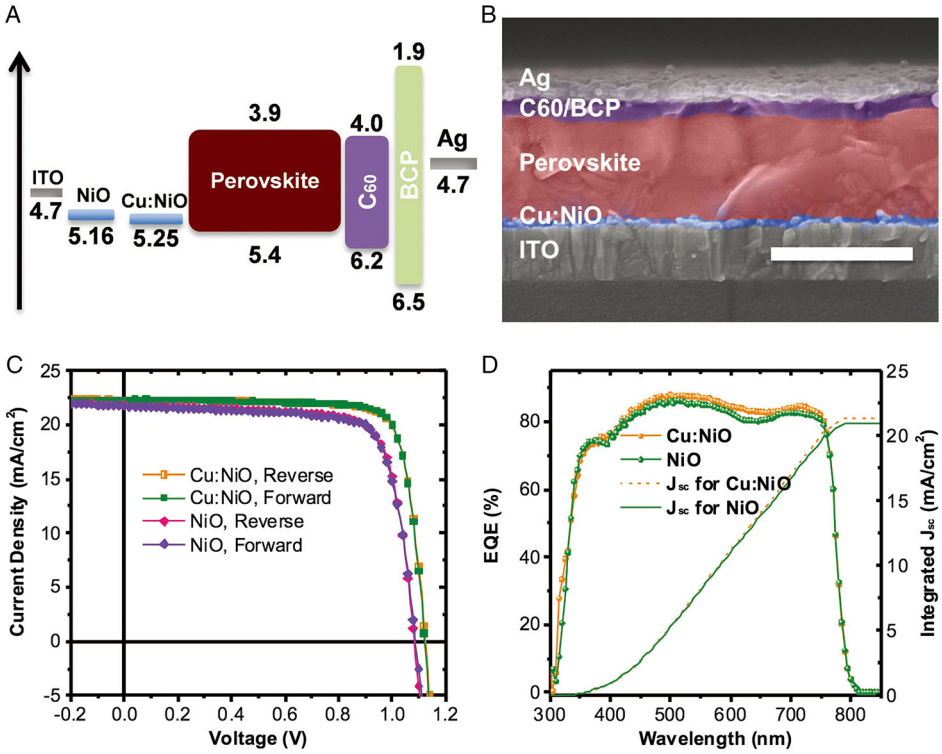

Figure 5. Typical p–i–n structure (Cu: NiO_x) device performance. A) Schematic diagram of energy levels at the inverted PSCs, B) cross-section SEM image of an inverted PSC with Cu: NiO HTL (scale bar: 500 nm), C) current–voltage characteristics of the optimal NiO and Cu: NiO-based inverted PSCs at the reverse and forward scan condition, and D) external quantum efficiency spectra and integrated J_{sc} curves of the corresponding optimal NiO and Cu: NiO devices. Reproduced with permission.[52b] Copyright 2018, John Wiley and Sons.

spray-coated[16] on the substrate. rGO also can function as an interface layer[21,171] or a dopant.[172]

Jokar et al. solution-processed GO and rGO HTL and get the best PCE of 13.8% and 16.4%.[94]Ahn et al. transferred CNTs film onto the perovskite layer and obtained a PCE of 13.2%, which can maintain 80% after 2200 h in ambient air under glass sealing. Habisreutinger et al. spin-coated P3HT/SWNTs-PMMA layer as a resulting PCE of 15.3%, remaining 85% of the initial PCE after 96 h exposure to a temperature of 80 °C in air.[95]

3.3. Nickel Oxide (NiO_x): NiO

NiO_x or NiO HTL can be produced by spin-coating. Some researchers spin-coated nickel-based precursors (i.e., nickel formate,[80] nickel(II) acetylacetonate,[84b] nickel acetate tetrahydrate,[173] nickel nitrate hexahydrate,[174] etc.) and then heated at high temperature (around 300°–500°) to form high transparency and high crystallinity NiO_x,[80,84b,161,173,174] which is an obvious drawback. Some researchers spin-coated or drop-casted NiO_x ink (dispersing synthesized NiO_x nanoparticles in deionized water /isopropyl alcohol solvents) and annealed it at low temperature (around 70°–130°) to remove the solvents.[52b,78,79a] Yin et al. received a preliminary PCE of 13.43% for flexible PSCs and 16.47% for rigid PSCs.[79] There are some other methods, such as spray pyrolysis (nickel-based precursor was sprayed and annealed at a high temperature of 500 °C with the best PCE of 13.49%),[83] doctor blade,[82] sol–gel-process[84b] (sol–gel with a size of 10–20 nm nanocrystalline was made from Nickel (II) acetylacetonate at 150°, spin-coated and annealed at 500° to form 30–40 nm film, PEC = 9.11%.), PLD (100 nm highly transparent, nanostructured NiO films was formed. The NiO ceramic target, which ablates the NiO material in the form of a plasma plume by a focused pulsed laser, is subsequently annealed at 200 °C for 1 h, in air. In 450–750 nm, optical transparency is 70–80%. The best PCE is 17.3%),[85] ALD (5–7.5 nm ultra-thin and un-doped NiO films were produced with the best PCE up to 16.40% with negligible hysteresis.),[84a] and e-beam evaporation[79b] (It is a low-temperature deposition process and applicable over large areas. The transparency is 65–90% in 400–800 nm. The highest efficiency is 15.4%),[79b] screen-print[81] (NiO paste is heated at 500 °C with PCE of up to 15.03%), magnetron sputter[51] (the oxygen flow ratio has significant influences on the p-type characteristics and doping concentrations. It is a low-temperature sputter. Moreover, with adequate oxygen doping, the photovoltaic performance of the device could be further enhanced.), and electrodeposition[161] (the samples were annealed at 350 °C to form 100 nm thick film. The films appeared nonporous but with high surface roughness.), etc.

In p–i–n structure, Chen et al. doped 2,2'-(perfluoronaphthalene-2,6-diylidene)dimalononitrile (F6TCNNQ) as an effective *p*-type molecular dopant to increase both VBM and Fermi levels of NiO_x HTLs, as well as upgrade the conductivity of NiO_x film by increasing hole concentration inside. As a result, the best PCE is increased from 16.47% to 20.86% compared with pristine NiO_x.[78a] Similarly, Chen et al. doped Cu in NiO to increase the best PCE from 18.18% to 20.26% and the former maintain ≈95% PCE after 1000 h when encapsulated in the ambient environment (**Figure 5**).[52b] Cu: NiO devices show high efficiency, with the best PCE of 20.26% on rigid and 17.41% on flexible substrates.[52b]

3.4. Other Transition Metal Oxides

Sun et al. spin-coated VO_x sols received the best PCE of 14.23%. (In the range of 500–900 nm, the VO_x layers present an extremely high transmittance of 95–98%, while in the wavelength range of 300–500 nm, the transmittance slightly decreased to 75%.)[91b] Shalan et al. used the spin-coating CoO_x method to achieve a PCE of 14.5%.[91c]

4. Cost

Different HTMs may vary in their approaches to film depositions. For the sake of cost comparison, all the HTLs use the method of spin-coating or printing a solution containing HTM nanocrystals to estimate the cost, even though these two methods are not the most convenient or low-cost ways to manufacture the HTL for some HTMs.

The synthesis of nanocrystals requires precursors and hydrothermal processes. The price of the precursors (raw material) is estimated roughly by the price of the HTM (M_i). The cost of hydrothermal processes includes the heating equipment cost (oven or heating plate), centrifugal equipment cost (E_i), and utility (U_i). The spin-coating or printing process cost covers spin-coating or printing equipment (E_i) and utility (U_i). The area of PSC is A_i.

Table 3. Costs of inorganic transport materials.

		Sigma-Aldrich (CNY (¥)/g, purity)	Aladdin (CNY (¥)/g, purity)
Organic	Spiro-OMeTAD	4492.08 (99%)	
Cu-based	CuSCN	21.37–27.76 (99%)	0.34 (99%)
	CuI	15.38 (99.5%)	1.34 (99.5%)
	CuO_x	10.61 (mixture of CuO and Cu_2O)	
	Cu_2O	17.72 (97%), 53.83 (99.99%)	1.56 (99%)
	CuO	1.26–16.78 (98%)	0.51 (99%)
Ni-based	NiO	15.03 (99.8%)	0.89 (99.0%)
Other transition-metal-based	MoO_2	20.52 (99%)	2.91 (99%)
	MoO_3	11.38 (99.5%)	0.71 (99.5%)
	WO_3	7.59(99.9%)	1.28 (99.8%)
	CrO_3	12.13(98.0%), 20.98(99.0%)	0.29 (99%)
	Cr_2O_3	5.17(98.0%)	0.49 (99.0%)
	V_2O_3	21.56(98%)	
	V_2O_5	36.84(98%)	
	CoO	389.23(99.99%)	1.97 (AR)
Carbon-based	GO	60.74(paste)	1799.00 (98%)
	rGO	7,006.59(carbon 75%)	2207.00 (99%)
	SWCNT	401.80(carbon 85%)	2999.00 (95%)
	MWCNT	113.90(carbon 95%)	139 (99.9%)

The cost of the unit area is

$$C_{\text{area}} = \frac{\sum(M_i + E_i + U_i)}{\sum A_i} \quad (1)$$

If E_i and U_i are approximated in mass production, the cost comparison between different HTMs can be approximated and estimated by M_i. The cost list can be seen in **Table 3**.

5. Conclusion

Overall, this review summarizes the physical and chemical properties of inorganic *p*-type materials for HTLs and many advantages including excellent stability, high conductivity, low cost, etc. The various fabrication methods of HTLs are also discussed, with which the inorganic HTLs are widely applied in PSCs to achieve much progress in stability. In addition, inorganic HTLs also have simple fabrication processes and low fabrication costs compared to traditional organic HTLs, which make large-scale commercial production of PSCs possible. However, the low efficiency of inorganic HTL-based PSCs remains a problem and needs more effort.

Future efforts to improve the performance of inorganic HTL-based PSCs can be devoted to modifying the surfaces or inserting the interface layers. Modified surfaces or insert interface layers contribute to better energy alignment or reduced resistance at the HTL/perovskite or HTL/electrode interface, which minimizes the potential charge loss between interfaces. Another crucial access for PCE improvement is searching for suitable solvents that dissolve inorganic HTMs well but do not degrade the perovskite layer, which helps shape uniform solution-processed HTLs. Also, utilizing the high transmittance of some inorganic HTMs is beneficial to yielding bifacial PSCs or high light-absorption PSCs for special applications. In addition, searching for new and efficient inorganic HTMs is always a research direction.

Acknowledgements

The funding support from the National Key R&D Program of China (2021YFF0501900 and 2019YFE0123400) and the Tianjin Distinguished Young Scholar Fund (20JCJQJC00260) is acknowledged by J.L.

Conflict of Interest

The authors declare no conflict of interest.

Keywords

hole transport materials, inorganic materials, perovskite solar cells

Received: August 29, 2022
Revised: November 7, 2022
Published online:

[1] NREL, https://www.nrel.gov/pv/cell-efficiency.html (accessed: November 2022).
[2] M. A. Green, A. Ho-Baillie, H. J. Snaith, *Nat. Photonics* **2014**, *8*, 506.
[3] N.-G. Park, *Mater. Today* **2015**, *18*, 65.
[4] M. He, X. Pang, X. Liu, B. Jiang, Y. He, H. Snaith, Z. Lin, *Angew. Chem.* **2016**, *128*, 4352.
[5] A. Miyata, A. Mitioglu, P. Plochocka, O. Portugall, J. T.-W. Wang, S. D. Stranks, H. J. Snaith, R. J. Nicholas, *Nat. Phys.* **2015**, *11*, 582.
[6] Y. Zhao, A. M. Nardes, K. J. A. F. M. Zhu, *J. Phys. Chem. Lett.* **2014**, *5*, 490.
[7] C. S. Ponseca Jr, T. J. Savenije, M. Abdellah, K. Zheng, A. Yartsev, T. R. Pascher, T. Harlang, P. Chabera, T. Pullerits, A. Stepanov, *J. Am. Chem. Soc.* **2014**, *136*, 5189.
[8] M. Saliba, J. P. Correa-Baena, M. Grätzel, A. Hagfeldt, A. Abate, *Angew. Chem., Int. Ed.* **2018**, *57*, 2554.
[9] P. Roy, N. K. Sinha, S. Tiwari, A. Khare, *Sol. Energy* **2020**, *198*, 665.
[10] X. Yin, Z. Song, Z. Li, W. Tang, *Energy Environ. Sci.* **2020**, *13*, 4057.
[11] E. Sheibani, L. Yang, J. Zhang, *Sol. RRL* **2020**, *4*, 2000461.
[12] T. Niu, W. Zhu, Y. Zhang, Q. Xue, X. Jiao, Z. Wang, Y.-M. Xie, P. Li, R. Chen, F. Huang, *Joule* **2021**, *5*, 249.
[13] W. Zhou, Z. Wen, P. Gao, *Adv. Mater.* **2018**, *8*, 1702512.
[14] G. W. Kim, H. Choi, M. Kim, J. Lee, S. Y. Son, T. Park, *Adv. Mater.* **2020**, *10*, 1903403.
[15] Q. Wei, M. Mukaida, Y. Naitoh, T. Ishida, *Adv. Mater.* **2013**, *25*, 2831.
[16] A. L. Palma, L. Cinà, S. Pescetelli, A. Agresti, M. Raggio, R. Paolesse, F. Bonaccorso, A. Di Carlo, *Nano Energy* **2016**, *22*, 349.
[17] J. Liu, S. K. Pathak, N. Sakai, R. Sheng, S. Bai, Z. Wang, H. J. Snaith, *Adv. Mater. Interfaces* **2016**, *3*, 1600571.
[18] X. Li, J. Yang, Q. Jiang, H. Lai, S. Li, Y. Tan, Y. Chen, S. Li, *J. Mater. Chem. A* **2019**, *7*, 7065.
[19] A. Capasso, F. Matteocci, L. Najafi, M. Prato, J. Buha, L. Cinà, V. Pellegrini, A. D. Carlo, F. Bonaccorso, *Adv. Mater.* **2016**, *6*, 1600920.
[20] W. H. Nguyen, C. D. Bailie, E. L. Unger, M. D. McGehee, *J. Am. Chem. Soc.* **2014**, *136*, 10996.
[21] N. Arora, M. I. Dar, A. Hinderhofer, N. Pellet, F. Schreiber, S. M. Zakeeruddin, M. Grätzel, *Science* **2017**, *358*, 768.
[22] a) H. Zhang, H. Wang, W. Chen, A. K.-Y. Jen, *Adv. Mater.* **2017**, *29*, 1604984; b) Y. Chen, Z. Yang, X. Jia, Y. Wu, N. Yuan, J. Ding, W.-H. Zhang, S. Liu, *Nano Energy* **2019**, *61*, 148; c) I. T. Papadas, A. Savva, A. Ioakeimidis, P. Eleftheriou, G. S. Armatas, S. A. Choulis, *Mater. Today Energy* **2018**, *8*, 57; d) H. Zhang, H. Wang, H. Zhu, C.-C. Chueh, W. Chen, S. Yang, A. K.-Y. Jen, *Adv. Energy Mater.* **2018**, *8*, 1702762; e) S. Akin, F. Sadegh, S. Turan, S. Sonmezoglu, *ACS Appl. Mater. Interfaces* **2019**, *11*, 45142.
[23] P. Pattanasattayavong, G. O. N. Ndjawa, K. Zhao, K. W. Chou, N. Yaacobi-Gross, B. C. O'Regan, A. Amassian, T. D. Anthopoulos, *Chem. Commun.* **2013**, *49*, 4154.
[24] a) N. Yaacobi-Gross, N. D. Treat, P. Pattanasattayavong, H. Faber, A. K. Perumal, N. Stingelin, D. D. C. Bradley, P. N. Stavrinou, M. Heeney, T. D. Anthopoulos, *Adv. Energy Mater.* **2015**, *5*, 1401529; b) N. Wijeyasinghe, A. Regoutz, F. Eisner, T. Du, L. Tsetseris, Y.-H. Lin, H. Faber, P. Pattanasattayavong, J. Li, F. Yan, M. A. McLachlan, D. J. Payne, M. Heeney, T. D. Anthopoulos, *Adv. Funct. Mater.* **2017**, *27*, 1701818.
[25] H. Kawazoe, M. Yasukawa, H. Hyodo, M. Kurita, H. Yanagi, H. Hosono, *Nature* **1997**, *389*, 939.
[26] H. Yanagi, S.-I. Inoue, K. Ueda, H. Kawazoe, H. Hosono, N. Hamada, *J. Appl. Phys.* **2000**, *88*, 4159.
[27] Z. Q. Yao, B. He, L. Zhang, C. Q. Zhuang, T. W. Ng, S. L. Liu, M. Vogel, A. Kumar, W. J. Zhang, C. S. Lee, S. T. Lee, X. Jiang, *Appl. Phys. Lett.* **2012**, *100*, 062102.
[28] S. Gao, Y. Zhao, P. Gou, N. Chen, Y. Xie, *Nanotechnology* **2003**, *14*, 538.
[29] K. Ueda, T. Hase, H. Yanagi, H. Kawazoe, H. Hosono, H. Ohta, M. Orita, M. Hirano, *J. Appl. Phys.* **2001**, *89*, 1790.

[30] D. Xiong, Z. Xu, X. Zeng, W. Zhang, W. Chen, X. Xu, M. Wang, Y.-B. Cheng, *J. Mater. Chem.* **2012**, *22*, 24760.
[31] S. Nie, A. Liu, Y. Meng, B. Shin, G. Liu, F. Shan, *J. Mater. Chem. C* **2018**, *6*, 1393.
[32] H.-Y. Chen, J.-H. Wu, *Appl. Surf. Sci.* **2012**, *258*, 4844.
[33] B. A. Nejand, V. Ahmadi, S. Gharibzadeh, H. R. Shahverdi, *ChemSusChem* **2016**, *9*, 302.
[34] B. S. Li, K. Akimoto, A. Shen, *J. Cryst. Growth* **2009**, *311*, 1102.
[35] P.-K. Kung, M.-H. Li, P.-Y. Lin, Y.-H. Chiang, C.-R. Chan, T.-F. Guo, P. Chen, *Adv. Mater. Interfaces* **2018**, *5*, 1800882.
[36] B. Gil, A. J. Yun, Y. Lee, J. Kim, B. Lee, B. Park, *Electron. Mater. Lett.* **2019**, *15*, 505.
[37] Z. H. Bakr, Q. Wali, A. Fakharuddin, L. Schmidt-Mende, T. M. Brown, R. Jose, *Nano Energy* **2017**, *34*, 271.
[38] M. Zi, J. Li, Z. Zhang, X. Wang, J. Han, X. Yang, Z. Qiu, H. Gong, Z. Ji, B. Cao, *Phys. Status Solidi (A)* **2015**, *212*, 1466.
[39] F.-L. Schein, H. V. Wenckstern, M. Grundmann, *Appl. Phys. Lett.* **2013**, *102*, 092109.
[40] S. Inudo, M. Miyake, T. Hirato, *Phys. Status Solidi (A)* **2013**, *210*, 2395.
[41] D. Chen, Y. Wang, Z. Lin, J. Huang, X. Chen, D. Pan, F. Huang, *Cryst. Growth Des.* **2010**, *10*, 2057.
[42] A. Tang, J. Liu, J. Ji, M. Dou, Z. Li, F. Wang, *Appl. Surf. Sci.* **2016**, *383*, 253.
[43] L. S. Khanzada, I. Levchuk, Y. Hou, H. Azimi, A. Osvet, R. Ahmad, M. Brandl, P. Herre, M. Distaso, R. Hock, W. Peukert, M. Batentschuk, C. J. Brabec, *Adv. Funct. Mater.* **2016**, *26*, 8300.
[44] J. Ge, P. Koirala, C. R. Grice, P. J. Roland, Y. Yu, X. Tan, R. J. Ellingson, R. W. Collins, Y. Yan, *Adv. Mater.* **2017**, *7*, 1601803.
[45] Z. Chen, K. Sun, Z. Su, F. Liu, D. Tang, H. Xiao, L. Shi, L. Jiang, X. Hao, Y. Lai, *ACS Appl. Energy Mater.* **2018**, *1*, 3420.
[46] J. Xie, Q. Yi, F. Zhang, R. Bagheri, F. Zheng, G. Zou, *ACS Appl. Mater. Interfaces* **2019**, *11*, 33102.
[47] H. Guo, C. Ma, Z. Chen, X. Jia, Q. Cang, N. Yuan, J. Ding, *Sol. Energy* **2019**, *181*, 301.
[48] R. Teimouri, R. Mohammadpour, *Superlattices Microstruct.* **2018**, *118*, 116.
[49] W. Ke, D. Zhao, C. R. Grice, A. J. Cimaroli, G. Fang, Y. Yan, *J. Mater. Chem. A* **2015**, *3*, 23888.
[50] H. Lei, G. Yang, X. Zheng, Z.-G. Zhang, C. Chen, J. Ma, Y. Guo, Z. Chen, P. Qin, Y. Li, G. Fang, *Sol. RRL* **2017**, *1*, 1700038.
[51] K.-C. Wang, P.-S. Shen, M.-H. Li, S. Chen, M.-W. Lin, P. Chen, T.-F. Guo, *ACS Appl. Mater. Interfaces* **2014**, *6*, 11851.
[52] a) S. Yue, K. Liu, R. Xu, M. Li, M. Azam, K. Ren, J. Liu, Y. Sun, Z. Wang, D. Cao, X. Yan, S. Qu, Y. Lei, Z. Wang, *Energy Environ. Sci.* **2017**, *10*, 2570; b) W. Chen, Y. Wu, J. Fan, A. B. Djurišić, F. Liu, H. W. Tam, A. Ng, C. Surya, W. K. Chan, D. Wang, Z.-B. He, *Adv. Energy Mater.* **2018**, *8*, 1703519.
[53] W.-Y. Chen, J.-S. Jeng, K.-L. Huang, J.-S. Chen, *J. Vac. Sci. Technol., A* **2013**, *31*, 021501.
[54] J. D. Hwang, T. H. Ho, *Mater. Sci. Semicond. Process.* **2017**, *71*, 396.
[55] S. C. Chen, T. Y. Kuo, Y. C. Lin, H. C. Lin, *Thin Solid Films* **2011**, *519*, 4944.
[56] M. Cheng, Y. Li, M. Safdari, C. Chen, P. Liu, L. Kloo, L. Sun, *Adv. Mater.* **2017**, *7*, 1602556.
[57] X. Gu, W. Cui, H. Li, Z. Wu, Z. Zeng, S.-T. Lee, H. Zhang, B. Sun, *Adv. Mater.* **2013**, *3*, 1262.
[58] N. M. Dissanayake, Z. Zhong, *Nano Lett.* **2011**, *11*, 286.
[59] D. Suh, D. Lee, C. Kang, I.-J. Shon, W. Kim, S. Baik, *J. Mater. Chem.* **2012**, *22*, 21376.
[60] S. Ye, W. Sun, Y. Li, W. Yan, H. Peng, Z. Bian, Z. Liu, C. Huang, *Nano Lett.* **2015**, *15*, 3723.
[61] P. Qin, S. Tanaka, S. Ito, N. Tetreault, K. Manabe, H. Nishino, M. K. Nazeeruddin, M. Grätzel, *Nat. Commun.* **2014**, *5*, 3834.
[62] M. Jung, Y. C. Kim, N. J. Jeon, W. S. Yang, J. Seo, J. H. Noh, S. Il Seok, *ChemSusChem* **2016**, *9*, 2592.
[63] A. Huang, L. Lei, Y. Yu, Y. Liu, S. Yang, S. Bao, X. Cao, P. Jin, *Nanotechnology* **2017**, *28*, 20LT02.
[64] W. Sun, S. Ye, H. Rao, Y. Li, Z. Liu, L. Xiao, Z. Chen, Z. Bian, C. Huang, *Nanoscale* **2016**, *8*, 15954.
[65] D. B. Khadka, Y. Shirai, M. Yanagida, K. Miyano, *Sol. Energy Mater. Sol. Cells* **2020**, *210*, 110486.
[66] a) H. Wang, Z. Yu, X. Jiang, J. Li, B. Cai, X. Yang, L. Sun, *Energy Technol.* **2017**, *5*, 1836; b) S. Gharibzadeh, B. A. Nejand, A. Moshaii, N. Mohammadian, A. H. Alizadeh, R. Mohammadpour, V. Ahmadi, A. Alizadeh, *ChemSusChem* **2016**, *9*, 1929; c) B. Abdollahi Nejand, P. Nazari, S. Gharibzadeh, V. Ahmadi, A. Moshaii, *Chem. Commun.* **2017**, *53*, 747.
[67] P. Nazari, F. Ansari, B. Abdollahi Nejand, V. Ahmadi, M. Payandeh, M. Salavati-Niasari, *J. Phys. Chem. C* **2017**, *121*, 21935.
[68] a) X. Li, J. Yang, Q. Jiang, W. Chu, D. Zhang, Z. Zhou, J. Xin, *ACS Appl. Mater. Interfaces* **2017**, *9*, 41354; b) M. Huangfu, Y. Shen, G. Zhu, K. Xu, M. Cao, F. Gu, L. Wang, *Appl. Surf. Sci.* **2015**, *357*, 2234.
[69] G. A. Sepalage, S. Meyer, A. Pascoe, A. D. Scully, F. Huang, U. Bach, Y.-B. Cheng, L. Spiccia, *Adv. Funct. Mater.* **2015**, *25*, 5650.
[70] S. Uthayaraj, D. G. B. C. Karunarathne, G. R. A. Kumara, T. Murugathas, S. Rasalingam, R. M. G. Rajapakse, P. Ravirajan, D. Velauthapillai, *Materials* **2019**, *12*, 2037.
[71] F. Igbari, M. Li, Y. Hu, Z.-K. Wang, L.-S. Liao, *J. Mater. Chem. A* **2016**, *4*, 1326.
[72] H. Zhang, H. Wang, W. Chen, A. K. Y. Jen, *Adv. Mater.* **2017**, *29*, 1604984.
[73] H. Rao, S. Ye, W. Sun, W. Yan, Y. Li, H. Peng, Z. Liu, Z. Bian, Y. Li, C. Huang, *Nano Energy* **2016**, *27*, 51.
[74] C. Zuo, L. Ding, *Small* **2015**, *11*, 5528.
[75] C. Liu, X. Zhou, S. Chen, X. Zhao, S. Dai, B. Xu, *Adv. Sci.* **2019**, *6*, 1801169.
[76] J. Ge, C. R. Grice, Y. Yan, *J. Mater. Chem. A* **2017**, *5*, 2920.
[77] Y. Zhang, Z. Zhang, Y. Liu, Y. Liu, H. Gao, Y. Mao, *Org. Electron.* **2019**, *67*, 168.
[78] a) W. Chen, Y. Zhou, L. Wang, Y. Wu, B. Tu, B. Yu, F. Liu, H.-W. Tam, G. Wang, A. B. Djurišić, L. Huang, Z. He, *Adv. Mater.* **2018**, *30*, 1800515; b) Y. Yang, H. Chen, X. Zheng, X. Meng, T. Zhang, C. Hu, Y. Bai, S. Xiao, S. Yang, *Nano Energy* **2017**, *42*, 322.
[79] a) X. Yin, P. Chen, M. Que, Y. Xing, W. Que, C. Niu, J. Shao, *ACS Nano* **2016**, *10*, 3630; b) S. R. Pae, S. Byun, J. Kim, M. Kim, I. Gereige, B. Shin, *ACS Appl. Mater. Interfaces* **2018**, *10*, 534.
[80] K.-C. Wang, J.-Y. Jeng, P.-S. Shen, Y.-C. Chang, E. W.-G. Diau, C.-H. Tsai, T.-Y. Chao, H.-C. Hsu, P.-Y. Lin, P. Chen, T.-F. Guo, T.-C. Wen, *Sci. Rep.* **2014**, *4*, 4756.
[81] K. Cao, Z. Zuo, J. Cui, Y. Shen, T. Moehl, S. M. Zakeeruddin, M. Grätzel, M. Wang, *Nano Energy* **2015**, *17*, 171.
[82] X. Xu, Z. Liu, Z. Zuo, M. Zhang, Z. Zhao, Y. Shen, H. Zhou, Q. Chen, Y. Yang, M. Wang, *Nano Lett.* **2015**, *15*, 2402.
[83] W. Chen, Y. Wu, J. Liu, C. Qin, X. Yang, A. Islam, Y.-B. Cheng, L. Han, *Energy Environ. Sci.* **2015**, *8*, 629.
[84] a) S. Seo, I. J. Park, M. Kim, S. Lee, C. Bae, H. S. Jung, N.-G. Park, J. Y. Kim, H. Shin, *Nanoscale* **2016**, *8*, 11403; b) Z. Zhu, Y. Bai, T. Zhang, Z. Liu, X. Long, Z. Wei, Z. Wang, L. Zhang, J. Wang, F. Yan, S. Yang, *Angew. Chem., Int. Ed.* **2014**, *53*, 12571.
[85] J. H. Park, J. Seo, S. Park, S. S. Shin, Y. C. Kim, N. J. Jeon, H.-W. Shin, T. K. Ahn, J. H. Noh, S. C. Yoon, C. S. Hwang, S. I. Seok, *Adv. Mater.* **2015**, *27*, 4013.
[86] F. Xie, C.-C. Chen, Y. Wu, X. Li, M. Cai, X. Liu, X. Yang, L. Han, *Energy Environ. Sci.* **2017**, *10*, 1942.
[87] W. Chen, Y. Wu, Y. Yue, J. Liu, W. Zhang, X. Yang, H. Chen, E. Bi, I. Ashraful, M. Grätzel, L. Han, *Science* **2015**, *350*, 944.

[88] W. Chen, F.-Z. Liu, X.-Y. Feng, A. B. Djurišić, W. K. Chan, Z.-B. He, *Adv. Mater.* **2017**, *7*, 1700722.
[89] C. Liu, W. Li, J. Chen, J. Fan, Y. Mai, R. E. I. Schropp, *Nano Energy* **2017**, *41*, 75.
[90] K. Im, J. H. Heo, S. H. Im, J. Kim, *Chem. Eng. J.* **2017**, *330*, 698.
[91] a) Z.-L. Tseng, L.-C. Chen, C.-H. Chiang, S.-H. Chang, C.-C. Chen, C.-G. Wu, *Sol. Energy* **2016**, *139*, 484; b) H. Sun, X. Hou, Q. Wei, H. Liu, K. Yang, W. Wang, Q. An, Y. Rong, *Chem. Commun.* **2016**, *52*, 8099; c) A. E. Shalan, T. Oshikiri, S. Narra, M. M. Elshanawany, K. Ueno, H.-P. Wu, K. Nakamura, X. Shi, E. W.-G. Diau, H. Misawa, *ACS Appl. Mater. Interfaces* **2016**, *8*, 33592.
[92] P.-L. Qin, H.-W. Lei, X.-L. Zheng, Q. Liu, H. Tao, G. Yang, W.-J. Ke, L.-B. Xiong, M.-C. Qin, X.-Z. Zhao, G.-J. Fang, *Adv. Mater. Interfaces* **2016**, *3*, 1500799.
[93] P. Qin, Q. He, G. Yang, X. Yu, L. Xiong, G. Fang, *Surf. Interfaces* **2018**, *10*, 93.
[94] E. Jokar, Z. Y. Huang, S. Narra, C.-Y. Wang, V. Kattoor, C.-C. Chung, E. W.-G. Diau, *Adv. Mater.* **2018**, *8*, 1701640.
[95] S. N. Habisreutinger, T. Leijtens, G. E. Eperon, S. D. Stranks, R. J. Nicholas, H. J. Snaith, *Nano Lett.* **2014**, *14*, 5561.
[96] a) K. Aitola, K. Domanski, J.-P. Correa-Baena, K. Sveinbjörnsson, M. Saliba, A. Abate, M. Grätzel, E. Kauppinen, E. M. J. Johansson, W. Tress, A. Hagfeldt, G. Boschloo, *Adv. Mater.* **2017**, *29*, 1606398; b) K. Aitola, K. Sveinbjörnsson, J.-P. Correa-Baena, A. Kaskela, A. Abate, Y. Tian, E. M. J. Johansson, M. Grätzel, E. I. Kauppinen, A. Hagfeldt, G. Boschloo, *Energy Environ. Sci.* **2016**, *9*, 461.
[97] Z. Wei, H. Chen, K. Yan, X. Zheng, S. Yang, *J. Mater. Chem. A* **2015**, *3*, 24226.
[98] S. Gholipour, J.-P. Correa-Baena, K. Domanski, T. Matsui, L. Steier, F. Giordano, F. Tajabadi, W. Tress, M. Saliba, A. Abate, A. Morteza Ali, N. Taghavinia, M. Grätzel, A. Hagfeldt, *Adv. Mater.* **2016**, *6*, 1601116.
[99] a) T. Malinauskas, D. Tomkute-Luksiene, R. Sens, M. Daskeviciene, R. Send, H. Wonneberger, V. Jankauskas, I. Bruder, V. Getautis, *ACS Appl. Mater. Interfaces* **2015**, *7*, 11107; b) I. S. Yang, M. R. Sohn, S. D. Sung, Y. J. Kim, Y. J. Yoo, J. Kim, W. I. Lee, *Nano Energy* **2017**, *32*, 414.
[100] X. Zhao, H.-S. Kim, J.-Y. Seo, N.-G. Park, *ACS Appl. Mater. Interfaces* **2017**, *9*, 7148.
[101] a) S. Kim, S. Bae, S.-W. Lee, K. Cho, K. D. Lee, H. Kim, S. Park, G. Kwon, S.-W. Ahn, H.-M. Lee, Y. Kang, H.-S. Lee, D. Kim, *Sci. Rep.* **2017**, *7*, 1200; b) J. Yang, B. D. Siempelkamp, D. Liu, T. L. Kelly, *ACS Nano* **2015**, *9*, 1955.
[102] J. Luo, J. Xia, H. Yang, L. Chen, Z. Wan, F. Han, H. A. Malik, X. Zhu, C. Jia, *Energy Environ. Sci.* **2018**, *11*, 2035.
[103] Y. Wang, L. Duan, M. Zhang, Z. Hameiri, X. Liu, Y. Bai, X. Hao, *Sol. RRL* **2022**, *6*, 2200234.
[104] Z. Yu, L. Sun, *Adv. Mater.* **2015**, *5*, 1500213.
[105] F. Li, X. Deng, F. Qi, Z. Li, D. Liu, D. Shen, M. Qin, S. Wu, F. Lin, S.-H. Jang, *J. Am. Chem. Soc.* **2020**, *142*, 20134.
[106] F. M. Rombach, S. A. Haque, T. J. Macdonald, *Energy Environ. Sci.* **2021**, *14*, 5161.
[107] I. Lee, N. Rolston, P.-L. Brunner, R. H. Dauskardt, *ACS Appl. Mater. Interfaces* **2019**, *11*, 23757.
[108] X. Jiang, Z. Yu, Y. Zhang, J. Lai, J. Li, G. G. Gurzadyan, X. Yang, L. Sun, *Sci. Rep.* **2017**, *7*, 42564.
[109] W.-Y. Chen, L.-L. Deng, S.-M. Dai, X. Wang, C.-B. Tian, X.-X. Zhan, S.-Y. Xie, R.-B. Huang, L.-S. Zheng, *J. Mater. Chem. A* **2015**, *3*, 19353.
[110] H. Elbohy, B. Bahrami, S. Mabrouk, K. M. Reza, A. Gurung, R. Pathak, M. Liang, Q. Qiao, K. Zhu, *Adv. Funct. Mater.* **2019**, *29*, 1806740.
[111] P. Vivo, J. K. Salunke, A. Priimagi, *Materials* **2017**, *10*, 1087.
[112] H. D. Pham, L. Xianqiang, W. Li, S. Manzhos, A. K. K. Kyaw, P. Sonar, *Energy Environ. Sci.* **2019**, *12*, 1177.
[113] M. Kabešová, M. Dunaj-jurčo, M. Serator, J. Gažo, J. Garaj, *Inorg. Chim. Acta* **1976**, *17*, 161.
[114] a) D. L. Smith, V. I. Saunders, *Acta Crystallogr., Sect. B* **1981**, *37*, 1807; b) D. L. Smith, V. I. Saunders, *Acta Crystallogr., Sect. B* **1982**, *38*, 907.
[115] W. Ji, G.-Q. Yue, F.-S. Ke, S. Wu, H.-B. Zhao, L.-Y. Chen, S.-Y. Wang, Y. Jia, *J. Korean Phys. Soc.* **2012**, *60*, 1253.
[116] V. P. S. Perera, M. K. I. Senevirathna, P. K. D. D. P. Pitigala, K. Tennakone, *Sol. Energy Mater. Sol. Cells* **2005**, *86*, 443.
[117] a) J. E. Jaffe, T. C. Kaspar, T. C. Droubay, T. Varga, M. E. Bowden, G. J. Exarhos, *J. Phys. Chem. C* **2010**, *114*, 9111; b) K. Tennakone, A. H. Jayatissa, C. A. N. Fernando, S. Wickramanayake, S. Punchihewa, L. K. Weerasena, W. D. R. Premasiri, *Phys. Status Solidi (A)* **1987**, *103*, 491.
[118] P. Pattanasattayavong, N. Yaacobi-Gross, K. Zhao, G. O. N. Ndjawa, J. Li, F. Yan, B. C. O'Regan, A. Amassian, T. D. Anthopoulos, *Adv. Mater.* **2013**, *25*, 1504.
[119] B. Ptaszyński, E. Skiba, J. Krystek, *Thermochim. Acta* **1998**, *319*, 75.
[120] a) C. Liu, W. Wu, K. Liu, M. Li, G. Hu, H. Xu, *CrystEngComm* **2012**, *14*, 6750; b) E. V. A. Premalal, G. R. R. A. Kumara, R. M. G. Rajapakse, M. Shimomura, K. Murakami, A. Konno, *Chem. Commun.* **2010**, *46*, 3360.
[121] L. Petti, P. Pattanasattayavong, Y.-H. Lin, N. Münzenrieder, G. Cantarella, N. Yaacobi-Gross, F. Yan, G. Tröster, T. D. Anthopoulos, *Appl. Phys. Lett.* **2017**, *110*, 113504.
[122] N. D. Treat, N. Yaacobi-Gross, H. Faber, A. K. Perumal, D. D. C. Bradley, N. Stingelin, T. D. Anthopoulos, *Appl. Phys. Lett.* **2015**, *107*, 013301.
[123] a) A. Perumal, H. Faber, N. Yaacobi-Gross, P. Pattanasattayavong, C. Burgess, S. Jha, M. A. McLachlan, P. N. Stavrinou, T. D. Anthopoulos, D. D. C. Bradley, *Adv. Mater.* **2015**, *27*, 93; b) L.-J. Xu, J.-Y. Wang, X.-F. Zhu, X.-C. Zeng, Z.-N. Chen, *Adv. Funct. Mater.* **2015**, *25*, 3033.
[124] K. Tennakone, S. Wickramanayaka, S. Basu, *Chem. Phys. Lett.* **1985**, *121*, 551.
[125] K. Tennakone, *J. Electrochem. Soc.* **1984**, *131*, 1574.
[126] D. A. Keen, S. Hull, *J. Phys.: Condens. Matter* **1995**, *7*, 5793.
[127] J. X. M. Zheng-Johansson, R. L. McGreevy, *Solid State Ionics* **1996**, *83*, 35.
[128] S. Miyake, S. Hoshino, T. Takenaka, *J. Phys. Soc. Jpn.* **1952**, *7*, 19.
[129] P. M. Sirimanne, M. Rusop, T. Shirata, T. Soga, T. Jimbo, *Chem. Phys. Lett.* **2002**, *366*, 485.
[130] S.-Q. Bai, I. H. K. Wong, M. Lin, D. J. Young, T. S. A. Hor, *Dalton Trans.* **2018**, *47*, 5564.
[131] A. H. Alami, M. Faraj, K. Aokal, A. Abu Hawili, M. Tawalbeh, D. Zhang, *Nanomaterials* **2020**, *10*, 784.
[132] C. Yang, D. Souchay, M. Kneiß, M. Bogner, H. M. Wei, M. Lorenz, O. Oeckler, G. Benstetter, Y. Q. Fu, M. Grundmann, *Nat. Commun.* **2017**, *8*, 16076.
[133] A. Crovetto, H. Hempel, M. Rusu, L. Choubrac, D. Kojda, K. Habicht, T. Unold, *ACS Appl. Mater. Interfaces* **2020**, *12*, 48741.
[134] D. Ahn, S.-H. Park, *Sci. Rep.* **2016**, *6*, 20718.
[135] Z. Yang, M. Wang, J. Ding, Z. Sun, L. Li, J. Huang, J. Liu, J. Shao, *ACS Appl. Mater. Interfaces* **2015**, *7*, 21235.
[136] a) I. Konovalov, R. Szargan, *Appl. Phys. Lett.* **2003**, *82*, 2088; b) I. Konovalov, *Thin Solid Films* **2004**, *451–452*, 413.
[137] a) S. A. Mohamed, J. Gasiorowski, K. Hingerl, D. R. T. Zahn, M. C. Scharber, S. S. A. Obayya, M. K. El-Mansy, N. S. Sariciftci, D. A. M. Egbe, P. Stadler, *Sol. Energy Mater. Sol. Cells* **2015**, *143*,

369; b) K. Zhao, G. O. Ngongang Ndjawa, L. K. Jagadamma, A. E. Labban, H. Hu, Q. Wang, R. Li, M. Abdelsamie, P. M. Beaujuge, A. Amassian, *Nano Energy* **2015**, *16*, 458.
[138] K. Tennakone, G. R. R. A. Kumara, A. R. Kumarasinghe, K. G. U. Wijayantha, P. M. Sirimanne, *Semicond. Sci. Technol.* **1995**, *10*, 1689.
[139] S. Lany, J. Osorio-Guillén, A. Zunger, *Phys. Rev. B* **2007**, *75*, 241203.
[140] A. Corani, M.-H. Li, P.-S. Shen, P. Chen, T.-F. Guo, A. El Nahhas, K. Zheng, A. Yartsev, V. Sundström, C. S. Ponseca, *J. Phys. Chem. Lett.* **2016**, *7*, 1096.
[141] P. Qin, G. Fang, N. Sun, X. Fan, Q. Zheng, F. Chen, J. Wan, X. Zhao, *Thin Solid Films* **2011**, *519*, 4334.
[142] M. Kaltenbrunner, G. Adam, E. D. Głowacki, M. Drack, R. Schwödiauer, L. Leonat, D. H. Apaydin, H. Groiss, M. C. Scharber, M. S. White, N. S. Sariciftci, S. Bauer, *Nat. Mater.* **2015**, *14*, 1032.
[143] S. Murase, Y. Yang, *Adv. Mater.* **2012**, *24*, 2459.
[144] H. Peng, W. Sun, Y. Li, S. Ye, H. Rao, W. Yan, H. Zhou, Z. Bian, C. Huang, *Nano Res.* **2016**, *9*, 2960.
[145] S. Chu, R. Zhao, R. Liu, Y. Gao, X. Wang, C. Liu, J. Chen, H. Zhou, *Semicond. Sci. Technol.* **2018**, *33*, 115016.
[146] a) S. Pitchaiya, M. Natarajan, A. Santhanam, V. Asokan, A. Yuvapragasam, V. Madurai Ramakrishnan, S. E. Palanisamy, S. Sundaram, D. Velauthapillai, *Arabian J. Chem.* **2020**, *13*, 2526; b) P. Jiang, T. W. Jones, N. W. Duffy, K. F. Anderson, R. Bennett, M. Grigore, P. Marvig, Y. Xiong, T. Liu, Y. Sheng, L. Hong, X. Hou, M. Duan, Y. Hu, Y. Rong, G. J. Wilson, H. Han, *Carbon* **2018**, *129*, 830.
[147] C.-H. Chen, S. Hu, J.-F. Shih, C.-Y. Yang, Y.-W. Luo, R.-H. Jhang, C.-M. Chiang, Y. Hung Jr., *Sci. Rep.* **2017**, *7*, 3908.
[148] X. Gong, G. Liu, Y. Li, D. Y. W. Yu, W. Y. Teoh, *Chem. Mater.* **2016**, *28*, 8082.
[149] J. V. Milić, N. Arora, M. I. Dar, S. M. Zakeeruddin, M. Grätzel, *Adv. Mater. Interfaces* **2018**, *5*, 1800416.
[150] A. Agresti, S. Pescetelli, B. Taheri, A. E. Del Rio Castillo, L. Cinà, F. Bonaccorso, A. Di Carlo, *ChemSusChem* **2016**, *9*, 2609.
[151] Q. Zheng, Z. Li, J. Yang, J.-K. Kim, *Prog. Mater. Sci.* **2014**, *64*, 200.
[152] Y. Zhu, S. Murali, W. Cai, X. Li, J. W. Suk, J. R. Potts, R. S. Ruoff, *Adv. Mater.* **2010**, *22*, 3906.
[153] X.-M. Huang, L.-Z. Liu, S. Zhou, J.-J. Zhao, *Front. Phys.* **2020**, *15*, 33301.
[154] X.-Z. Tang, W. Li, Z.-Z. Yu, M. A. Rafiee, J. Rafiee, F. Yavari, N. Koratkar, *Carbon* **2011**, *49*, 1258.
[155] S. Stankovich, D. A. Dikin, R. D. Piner, K. A. Kohlhaas, A. Kleinhammes, Y. Jia, Y. Wu, S. T. Nguyen, R. S. Ruoff, *Carbon* **2007**, *45*, 1558.
[156] S. N. Habisreutinger, R. J. Nicholas, H. J. Snaith, *Adv. Mater.* **2017**, *7*, 1601839.
[157] J. Lee, M. M. Menamparambath, J.-Y. Hwang, S. Baik, *ChemSusChem* **2015**, *8*, 2358.
[158] R. Ihly, A.-M. Dowgiallo, M. Yang, P. Schulz, N. J. Stanton, O. G. Reid, A. J. Ferguson, K. Zhu, J. J. Berry, J. L. Blackburn, *Energy Environ. Sci.* **2016**, *9*, 1439.
[159] a) B. R. Sankapal, E. Goncalves, A. Ennaoui, M. C. Lux-Steiner, *Thin Solid Films* **2004**, *451–452*, 128; b) X.-D. Gao, X.-M. Li, W.-D. Yu, J.-J. Qiu, X.-Y. Gan, *Thin Solid Films* **2008**, *517*, 554.
[160] X. Zhang, S. Yoshioka, N. Loew, M. Ihara, *ECS Trans.* **2014**, *64*, 1.
[161] A. S. Subbiah, A. Halder, S. Ghosh, N. Mahuli, G. Hodes, S. K. Sarkar, *J. Phys. Chem. Lett.* **2014**, *5*, 1748.
[162] a) S. Ye, H. Rao, W. Yan, Y. Li, W. Sun, H. Peng, Z. Liu, Z. Bian, Y. Li, C. Huang, *Adv. Mater.* **2016**, *28*, 9648; b) K. Zhao, R. Munir, B. Yan, Y. Yang, T. Kim, A. Amassian, *J. Mater. Chem. A* **2015**, *3*, 20554.
[163] C. Chappaz-Gillot, R. Salazar, S. Berson, V. Ivanova, *Electrochim. Acta* **2013**, *110*, 375.
[164] S. L. Dhere, S. S. Latthe, C. Kappenstein, S. K. Mukherjee, A. V. Rao, *Appl. Surf. Sci.* **2010**, *256*, 3967.
[165] H. Kang, R. Liu, K. Chen, Y. Zheng, Z. Xu, *Electrochim. Acta* **2010**, *55*, 8121.
[166] B. L. Zhu, X. Z. Zhao, *Phys. Status Solidi (A)* **2011**, *208*, 91.
[167] T. Tanaka, K. Kawabata, M. Hirose, *Thin Solid Films* **1996**, *281–282*, 179.
[168] a) W. Sun, Y. Li, S. Ye, H. Rao, W. Yan, H. Peng, Y. Li, Z. Liu, S. Wang, Z. Chen, L. Xiao, Z. Bian, C. Huang, *Nanoscale* **2016**, *8*, 10806; b) Z.-K. Yu, W.-F. Fu, W.-Q. Liu, Z.-Q. Zhang, Y.-J. Liu, J.-L. Yan, T. Ye, W.-T. Yang, H.-Y. Li, H.-Z. Chen, *Chin. Chem. Lett.* **2017**, *28*, 13; c) S. Chatterjee, A. J. Pal, *J. Phys. Chem. C* **2016**, *120*, 1428.
[169] H. Li, K. Cao, J. Cui, S. Liu, X. Qiao, Y. Shen, M. Wang, *Nanoscale* **2016**, *8*, 6379.
[170] a) J.-S. Yeo, R. Kang, S. Lee, Y.-J. Jeon, N. Myoung, C.-L. Lee, D.-Y. Kim, J.-M. Yun, Y.-H. Seo, S.-S. Kim, S.-I. Na, *Nano Energy* **2015**, *12*, 96; b) Z. Wu, S. Bai, J. Xiang, Z. Yuan, Y. Yang, W. Cui, X. Gao, Z. Liu, Y. Jin, B. Sun, *Nanoscale* **2014**, *6*, 10505.
[171] a) W. Li, H. Dong, X. Guo, N. Li, J. Li, G. Niu, L. Wang, *J. Mater. Chem. A* **2014**, *2*, 20105; b) H. Li, L. Tao, F. Huang, Q. Sun, X. Zhao, J. Han, Y. Shen, M. Wang, *ACS Appl. Mater. Interfaces* **2017**, *9*, 38967.
[172] a) K. T. Cho, G. Grancini, Y. Lee, D. Konios, S. Paek, E. Kymakis, M. K. Nazeeruddin, *ChemSusChem* **2016**, *9*, 3040; b) T. Gatti, S. Casaluci, M. Prato, M. Salerno, F. Di Stasio, A. Ansaldo, E. Menna, A. Di Carlo, F. Bonaccorso, *Adv. Funct. Mater.* **2016**, *26*, 7443; c) D.-Y. Lee, S.-I. Na, S.-S. Kim, *Nanoscale* **2016**, *8*, 1513.
[173] L. Hu, J. Peng, W. Wang, Z. Xia, J. Yuan, J. Lu, X. Huang, W. Ma, H. Song, W. Chen, Y.-B. Cheng, J. Tang, *ACS Photonics* **2014**, *1*, 547.
[174] X. Yin, Z. Yao, Q. Luo, X. Dai, Y. Zhou, Y. Zhang, Y. Zhou, S. Luo, J. Li, N. Wang, H. Lin, *ACS Appl. Mater. Interfaces* **2017**, *9*, 2439.

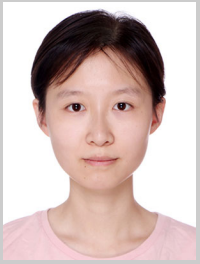

Xin Jing received her B.E. degree in material chemistry from Nankai University in 2019. She was a research assistant in the group Professor Jingshan Luo in Nankai University, working on inorganic hole-transporting layers for perovskite solar cells. Now, she is a master student in University of Michigan. Her interest is designing low-cost and high-efficiency perovskite solar cells.

Jingshan Luo is a full professor and vice director of the Institute of Photoelectronic Thin-Film Devices and Technology at Nankai University. He received his B.Sc degree in Jilin University in 2010 and his Ph.D. degree from Nanyang Technological University in 2014. After that, he went to École Polytechnique Fédérale de Lausanne (EPFL), Switzerland, for postdoctoral research in the laboratory of Professor Michael Grätzel, where he led the solar fuel subgroup. In 2018, he joined Nankai University. He has authored/coauthored more than 120 peer-reviewed publications, which have been cited more than 22,000 times with an H-index of 66. He has received many awards and honors, such as the MIT Technology Review TR35 in China, the 2018–2022 Highly Cited Researcher by Clarivate Analytics, and the Excellent Young Scholar Fund from National Science Foundation of China.